

Lined Circular Tunnels in Elastic Transversely Anisotropic Rock at Depth

Antonio Bobet

Received: 29 September 2009 / Accepted: 4 August 2010 / Published online: 1 October 2010
© Springer-Verlag 2010

Abstract Closed-form solutions for displacements and stresses of both the liner and the rock are presented for a deep circular tunnel excavated in transversely anisotropic rock above or below the water table subjected to static or seismic loading. The solutions are obtained with the assumption of elastic response of rock and liner, tied contact between rock and liner, impermeable liner, plane strain conditions along the tunnel axis and simultaneous excavation, and liner installation. The liner of a tunnel placed below the water table must support, in addition to the rock stresses, the full water pressure, while a tunnel located above the water table must support only the rock pressures. The solutions presented for static loading show, however, that displacements and stresses of the liner and rock are the same when the tunnel is placed above or below the water table as long as the total far-field stresses are the same. With rapid loading, e.g. seismic loading, excess pore pressures may be generated in saturated rock, which induce a different response than that of a tunnel excavated in dry rock. The analyses indicate that stresses and displacements are more uniform when excess pore pressures are produced, which seems to indicate that pore pressure generation tends to reduce non-uniform response in anisotropic rock.

Keywords Deep tunnel · Circular liner · Anisotropy · Transversely anisotropic rock · Water pressure · Undrained conditions

List of symbols

| | |
|---|---|
| A_s, I_s | Cross-section and moment of inertia of liner |
| E_x, E_y | Young's modulus of rock in x - and y -axis |
| E_s, ν_s | Young's modulus and Poisson's ratio of the liner |
| G_{xy} | Shear modulus of rock |
| k_x, k_y | Permeability of rock in x - and y -axis |
| M | Biot's modulus |
| p, q | Total mean stress and maximum shear stress of rock |
| r, θ | Polar coordinates |
| r_o | Radius of the tunnel |
| t | Liner thickness |
| T^s, M^s | Axial force and moment of liner |
| U_x, U_y | Displacement of the rock in cartesian coordinates |
| U_r, U_θ | Displacement of the rock in polar coordinates |
| U_r^s, U_θ^s | Displacement of the liner in polar coordinates |
| u | Pore pressures |
| u^{ff} | Pore pressure at far-field |
| x, y | Cartesian coordinates of axes of elastic symmetry |
| z | Complex number, $z_k = x + \mu_k y$, $k = 1, 2$ |
| α_x, α_y | Biot's constants in x - and y -axis |
| β | Angle of y -axis of elastic symmetry with far-field vertical stress |
| $\varepsilon_x, \varepsilon_y, \gamma$ | Axial and shear strains in x - and y -axis |
| μ_1, μ_2 | Roots of compatibility equation |
| $\nu_{xy}, \nu_{xz}, \nu_{yz}$ | Poisson's ratios of rock |
| $\sigma_v^{ff}, \sigma_h^{ff}, \tau^{ff}$ | Total normal and shear stresses at far-field |
| $\sigma_v, \sigma_h, \tau_{vh}$ | Total normal and shear stresses at far-field along axes of elastic symmetry |
| $\sigma_x, \sigma_y, \tau_{xy}$ | Total normal and shear stresses in Cartesian coordinate system |

A. Bobet (✉)
School of Civil Engineering, Purdue University,
West Lafayette, IN, USA
e-mail: bobet@purdue.edu

| | |
|---------------------------------------|---|
| $\sigma'_x, \sigma'_y, \sigma'_z$ | Effective normal stresses in Cartesian coordinate system |
| $\sigma_r, \sigma_\theta, \tau$ | Total radial, tangential, and shear stresses in polar coordinate system |
| $\sigma_r^s, \sigma_\theta^s, \tau^s$ | Stresses of the liner in polar coordinates |
| ζ | Change of fluid volume per unit volume of ground |

1 Introduction

The analysis of rock and liner stresses due to tunnel construction is often made with the assumption of homogeneous and isotropic rock. While the assumption has facilitated the development of closed-form solutions and has helped with the understanding of the fundamental mechanisms of rock–water–liner interaction, it is limited to sites where the rock is uniform. Tunnels may be built in formations where the properties of the rock are not isotropic. Typical examples include sedimentary and metamorphic foliated rocks. Stresses and deformations in the rock and loads in the liner differ from those obtained under the assumption of isotropic properties and strongly depend on the orientation of bedding or foliation with the tunnel axis (Hefny and Lo 1999; Tonon and Amadei 2002).

Work has been devoted to the analysis of rock–liner interaction for shallow or deep tunnels in dry ground (Peck 1969; Einstein and Schwartz 1979) or below the water table (Fernández et al. 1994; Bobet 2001, 2007, 2009a; Nam and Bobet 2006; Lee et al. 2006; Bobet and Nam 2007; Carranza-Torres and Zhao 2009), for elastic (Verruijt 1997, 1998; Verruijt and Booker 1996; Strack and Verruijt 2002; Exadaktylos and Stavropoulou 2002), poro-elastic (Wang 1996, 2000), plastic (Carranza-Torres and Fairhurst 2000; Sharan 2003, 2005; Carranza-Torres 2004) and poro-plastic rock (Giraud et al. 2002; Bobet 2009a), and for static and dynamic loading conditions (Wang 1993; Penzien 2000; Bobet 2003, 2009b; Huo et al. 2006; Bobet et al. 2008). Closed-form solutions are obtained in the previous work considering isotropic properties of the rock. There are, however, fundamental differences in behavior when the rock is anisotropic. Figure 1 can be used to illustrate some of the differences when a tunnel is excavated in isotropic or in anisotropic media. When the rock is isotropic, there are two axes of symmetry (Fig. 1a), each along the direction of far-field loading (note that the far-field loading can always be expressed in terms of the principal stress directions even if along vertical and horizontal planes there is shear). It is thus expected that the largest convergence and axial force and bending moment in the liner occur along the axes of symmetry. Stresses and deformations in the rock and liner depend on the magnitude of the far-field stresses, size of the

tunnel, and on the relative stiffness between the rock and the liner (e.g. Einstein and Schwartz 1979). This is not the case for a tunnel excavated in anisotropic rock, where the axes of elastic symmetry may not coincide with the directions of the far-field loading, and thus maximum convergence and liner stresses will occur at locations that will depend on the magnitude of loading and on the direction of loading with respect to the planes of anisotropy, in addition to the anisotropic properties of the rock or size of tunnel.

This paper presents analytical solutions for the stresses and displacements for both rock and liner for deep circular tunnels placed in anisotropic rock below the water table. The solutions apply to rock with transverse anisotropy with the tunnel axis parallel to one of the axes of elastic symmetry, as shown in Fig. 2a, where the tunnel axis is parallel to the z -coordinate axis. The following assumptions are made: (1) the tunnel is deep and so far-field stresses can be assumed as uniform and the magnitude of the vertical stress can be taken

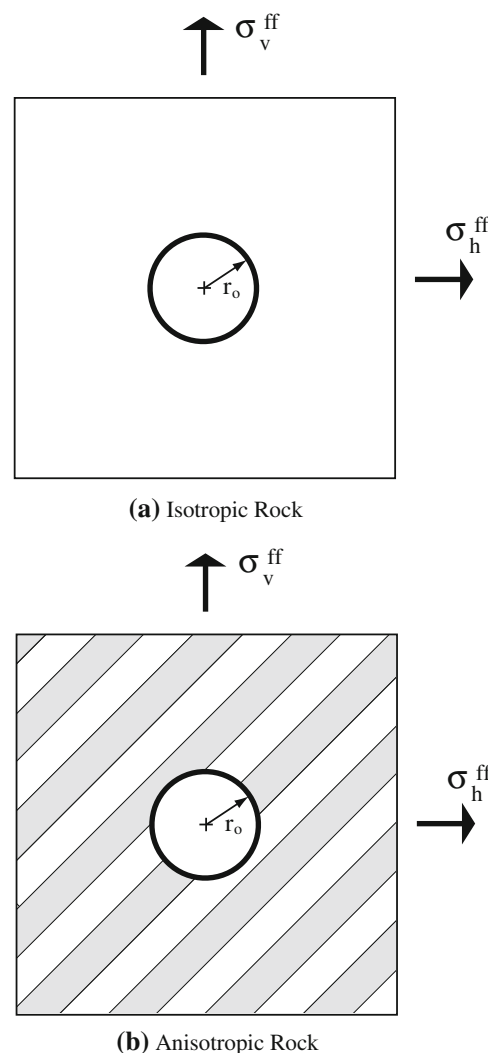
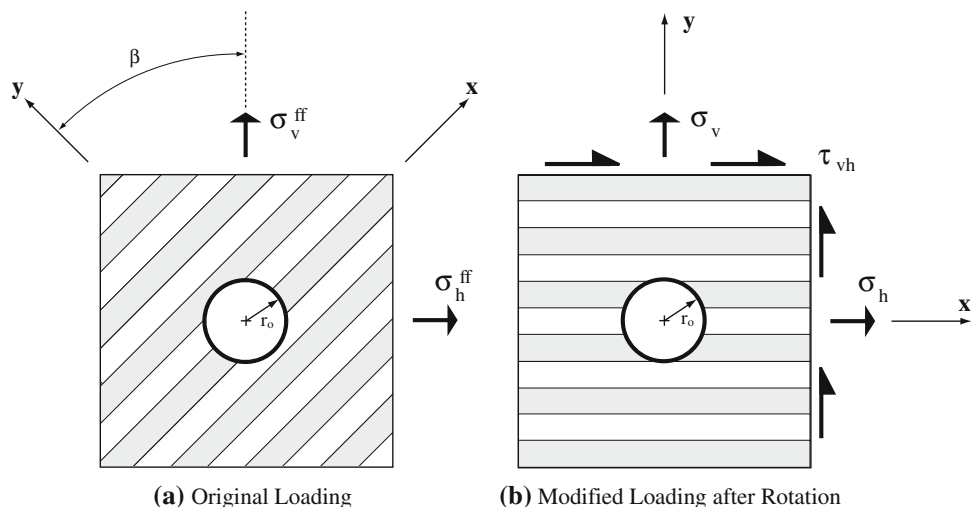


Fig. 1 Circular Tunnel

Fig. 2 Deep tunnel in transversely anisotropic rock



as the unit weight of the rock times the depth of the center of the tunnel; (2) the cross section of the tunnel is circular; (3) the rock is porous and elastic; (4) the rock has transverse anisotropy; (5) the liner is elastic and has a small thickness compared with the radius of the tunnel; (6) the contact between the liner and the rock is tied, i.e. there is no slip and the liner may not detach from the rock; and (7) plane strain conditions apply along the axis of the tunnel.

There are two scenarios of interest. The first one is that of a tunnel excavated below the water table with an impermeable liner and subjected to far-field gravity load. In this case, the pore pressures in the rock are uniform and equal to the ambient pore pressures. The second scenario is that of a tunnel below the water table, also with an impermeable liner, subjected to seismic loading. The seismic load is approximated with a quasi-static load in the form of a far-field shear stress. The fundamental difference between the two scenarios is that, for the seismic loading, the loading rate is considered fast such that excess pore pressures are generated and cannot dissipate during the duration of the loading, while for the other case, it is assumed that tunnel excavation occurs without generation of excess pore pressures. In all the analyses, tension is taken as positive and compression as negative, following the sign convention used in mechanics.

2 Poro-elasticity in Anisotropic Rock

The solution of any two-dimensional problem in poro-elasticity must satisfy the following conditions: equilibrium, constitutive model, strain compatibility, flow through the porous medium, and boundary conditions. The equations are expressed in the Cartesian coordinate system that coincides with the axes of elastic symmetry. Figure 2a shows the general problem of a tunnel excavated in transversely anisotropic

rock, where the axes of elastic symmetry make an angle β with the vertical axis. The problem is equivalent to that shown in Fig. 2b after a rotation of angle β . With the rotation the far-field stresses σ_v^{ff} and σ_h^{ff} transform into (Fig. 2b)

$$\begin{aligned} \sigma_v &= \frac{1}{2}(\sigma_v^{ff} + \sigma_h^{ff}) + \frac{1}{2}(\sigma_v^{ff} - \sigma_h^{ff}) \cos 2\beta \\ \sigma_h &= \frac{1}{2}(\sigma_v^{ff} + \sigma_h^{ff}) - \frac{1}{2}(\sigma_v^{ff} - \sigma_h^{ff}) \cos 2\beta \\ \tau_{vh} &= \frac{1}{2}(\sigma_v^{ff} - \sigma_h^{ff}) \sin 2\beta \end{aligned} \tag{1}$$

Equilibrium:

$$\begin{aligned} \frac{\partial \sigma_x}{\partial x} + \frac{\partial \tau_{xy}}{\partial y} &= 0 \\ \frac{\partial \sigma_y}{\partial y} + \frac{\partial \tau_{xy}}{\partial x} &= 0 \end{aligned} \tag{2}$$

where σ_x , σ_y , τ_{xy} are the total stresses along the x - and y -axis and the shear stresses, respectively, and x and y are the Cartesian coordinates.

The constitutive model is given by the equations of poro-elasticity, which in plane strain are given by (e.g. Detournay and Cheng 1993; Cheng 1998; Wang 2000)

$$\begin{aligned} \epsilon_x &= \alpha_1 \sigma'_x - \alpha_2 \sigma'_y \\ \epsilon_y &= -\alpha_2 \sigma'_x + \alpha_3 \sigma'_y \\ \gamma &= \frac{\tau_{xy}}{G_{xy}} \\ \sigma'_z &= \nu_{xz} \sigma'_x + \frac{E_x}{E_y} \nu_{yx} \sigma'_y \\ \alpha_1 &= \frac{1 - \nu_{xz}^2}{E_x} \\ \alpha_2 &= \frac{(1 + \nu_{xz}) \nu_{yx}}{E_y} \\ \alpha_3 &= \left(1 - \frac{E_x \nu_{yx}^2}{E_y}\right) \frac{1}{E_y} \end{aligned} \tag{3}$$

where σ'_x, σ'_y are the effective stresses in the x and y directions, E_x and E_y are the Young's modulus in the x and y directions, ν_{xz} and ν_{yx} are the Poisson's ratios in the xz and yx directions, respectively, and G_{xy} is the shear modulus. Note that because of the symmetry of the strain tensor, $\nu_{xy} = \nu_{yx} E_x/E_y$. Note also that the properties in the z and x directions are the same.

The relation between effective stresses and total stresses is

$$\begin{aligned}\sigma'_x &= \sigma_x + \alpha_x u \\ \sigma'_y &= \sigma_y + \alpha_y u\end{aligned}\quad (4)$$

where α_x and α_y are the Biot's constants in the x and y directions, and u is the pore pressure. Combining Eqs. 3 and 4 gives

$$\begin{aligned}\varepsilon_x &= \alpha_1 \sigma_x - \alpha_2 \sigma_y + \beta_1 u \\ \varepsilon_y &= -\alpha_2 \sigma_x + \alpha_3 \sigma_y + \beta_2 u \\ \gamma &= \frac{\tau_{xy}}{G_{xy}} \\ \beta_1 &= \alpha_1 \alpha_x - \alpha_2 \alpha_y \\ \beta_2 &= -\alpha_2 \alpha_x + \alpha_3 \alpha_y.\end{aligned}\quad (5)$$

Pore pressures must obey the following field equation

$$k_x \frac{\partial^2 u}{\partial x^2} + k_y \frac{\partial^2 u}{\partial y^2} = \gamma_w \frac{\partial \zeta}{\partial t}\quad (6)$$

where k_x and k_y are the permeabilities in the x and y axes, respectively, γ_w is the unit weight of the pore fluid, and ζ is the change of fluid volume per unit volume of the porous material. In addition,

$$u = M(\zeta - \alpha_x \varepsilon_x - \alpha_y \varepsilon_y)\quad (7)$$

where M is Biot's modulus, defined as the increase of the amount of fluid per unit volume of rock as a result of a unit increase of pore pressure under constant volumetric strain. For incompressible fluid and matrix and isotropic properties, i.e., for typical isotropic soils, $\alpha_x = \alpha_y = 1$ and $M \rightarrow \infty$.

Equilibrium equations can be satisfied if a stress function $F(x, y)$ is found such that (Lekhnitskii 1963)

$$\begin{aligned}\sigma_x &= \frac{\partial^2 F}{\partial y^2} \\ \sigma_y &= \frac{\partial^2 F}{\partial x^2} \\ \tau_{xy} &= -\frac{\partial^2 F}{\partial x \partial y}\end{aligned}\quad (8)$$

The compatibility equation can be written, in terms of the function $F(x, y)$ as

$$\alpha_1 \frac{\partial^4 F}{\partial y^4} + \alpha_3 \frac{\partial^4 F}{\partial x^4} + \left(\frac{1}{G_{xy}} - 2\alpha_2 \right) \frac{\partial^4 F}{\partial x^2 \partial y^2} = -\beta_1 \frac{\partial^2 u}{\partial y^2} - \beta_2 \frac{\partial^2 u}{\partial x^2}\quad (9)$$

The solution of Eq. 9 provides $F(x, y)$, and hence stresses and strains can be obtained from Eqs. 8 and 5. Lekhnitskii (1963) proposed a solution of Eq. 9 by introducing the complex variable $z_k = x + \mu_k y$, where μ_k is a complex number. Expressing Eq. 9 as a function of the complex variable z , one gets

$$\left[\alpha_1 \mu_k^4 + \left(\frac{1}{G_{xy}} - 2\alpha_2 \right) \mu_k^2 + \alpha_3 \right] \frac{\partial^4 F}{\partial z^4} = -\beta_1 \frac{\partial^2 u}{\partial y^2} - \beta_2 \frac{\partial^2 u}{\partial x^2}\quad (10)$$

By introducing the function $\phi(z_k) = F'(z_k) = \delta F / \delta z_k$, the stresses can be obtained from

$$\begin{aligned}\sigma_x &= 2\text{Re}[\mu_1^2 \phi_1'(z_1) + \mu_2^2 \phi_2'(z_2)] + \frac{\partial^2 F_o}{\partial y^2} \\ \sigma_y &= 2\text{Re}[\phi_1'(z_1) + \phi_2'(z_2)] + \frac{\partial^2 F_o}{\partial x^2} \\ \tau &= -2\text{Re}[\mu_1 \phi_1'(z_1) + \mu_2 \phi_2'(z_2)] - \frac{\partial^2 F_o}{\partial x \partial y}\end{aligned}\quad (11)$$

where F_o is a particular solution of Eq. 9 and μ_1 and μ_2 are the roots of the equation

$$\alpha_1 \mu_k^4 + \left(\frac{1}{G_{xy}} - 2\alpha_2 \right) \mu_k^2 + \alpha_3 = 0\quad (12)$$

Lekhnitskii (1963) showed that the roots are always complex numbers and are of the form

$$\begin{aligned}\mu_1 &= m_1 + i n_1 \\ \bar{\mu}_1 &= m_1 - i n_1 \\ \mu_2 &= m_2 + i n_2 \\ \bar{\mu}_2 &= m_2 - i n_2 \\ m_k &> 0 \\ i &= \sqrt{-1}\end{aligned}\quad (13)$$

3 Tunnel in Dry Rock or in Rock Below the Water Table with Impermeable Liner

3.1 General Formulation

For the case of a tunnel excavated in dry rock or below the water table, the pore pressures are either zero, for the case of dry ground, or are constant (i.e., given the assumption of deep tunnel, the ambient or far-field pore pressures are equal to the unit weight of water times the depth of the center of the tunnel below the water table). In either case,

the right-hand side of Eq. 10 is zero. The stress functions ϕ_1 and ϕ_2 , following Lekhnitskii's (1963) approach, are given by

$$\begin{aligned} \phi_1(z_1) &= \frac{1}{\mu_1 - \mu_2} \sum_{n=1}^{\infty} \frac{1}{2} (\bar{b}_n - \mu_2 \bar{a}_n) \zeta_1^{-n} \\ \phi_2(z_2) &= -\frac{1}{\mu_1 - \mu_2} \sum_{n=1}^{\infty} \frac{1}{2} (\bar{b}_n - \mu_1 \bar{a}_n) \zeta_2^{-n} \\ \sum_{n=1}^{\infty} \bar{a}_n e^{-n\theta i} &= \int (-\sigma_r \sin \theta - \tau \cos \theta) r_o d\theta \\ \sum_{n=1}^{\infty} \bar{b}_n e^{-n\theta i} &= \int (\sigma_r \cos \theta - \tau \sin \theta) r_o d\theta \\ z_k &= \frac{1}{2} (1 - \mu_k i) r_o \zeta_k + \frac{1}{2} (1 + \mu_k i) r_o \zeta_k^{-1} \end{aligned} \tag{14}$$

where ζ_k is a complex number that depends on z_k , as shown in the last expression in Eq. 14; \bar{a}_n and \bar{b}_n are the conjugates of the complex number a_n and b_n ; σ_r and τ the radial and shear stresses applied at the $r = r_o$ boundary; r_o is the radius of the tunnel. See Fig. 3. Note that the complex variable ζ_k at $r = r_o$ takes the form $\zeta_k = \cos \theta + i \sin \theta$ (see Fig. 3 for definition of coordinate θ).

Lekhnitskii's (1963) showed that μ_1 and μ_2 are complex numbers. It can be shown that they are pure imaginary numbers. From Eq. 12, it follows that

$$\begin{aligned} \mu_1^2 + \mu_2^2 &= \frac{2\alpha_2}{\alpha_1} - \frac{1}{\alpha_1 G_{xy}} \\ \mu_1^2 \mu_2^2 &= \frac{\alpha_3}{\alpha_1}, \quad \text{and so} \\ \mu_1^2 + \mu_2^2 - 2\mu_1 \mu_2 &= (\mu_1 - \mu_2)^2 \\ &= \frac{1}{\alpha_1} \left(-\frac{1}{G_{xy}} + 2\alpha_2 - 2\sqrt{\alpha_1 \alpha_3} \right) < 0 \end{aligned} \tag{15}$$

Note that $\alpha_1 \alpha_3 > \alpha_2^2$ so the compliance matrix, e.g., from the first two equations of Eq. 3, is positive definite. Hence, the expression in parentheses on the right-hand side of the last equation must be negative, and so $(\mu_1 - \mu_2)$ is an imaginary number. This results, from Eq. 13, in $m_1 = m_2$. Given that the result must hold for any possible elastic properties, and also that it must satisfy the two-first equations in Eq. 15, $m_1 = m_2 = 0$, and thus the roots of Eq. 12 are pure imaginary numbers.

3.2 Dry Rock

The problem of a tunnel in dry rock is solved first. In this case the pore pressures in the rock are zero, i.e., $u = 0$. The solution of a tunnel in transversely anisotropic dry rock and subjected to far-field stresses, as shown in Fig. 2b, can be decomposed into the following problems (see Fig. 4): I, no tunnel; II, no liner; III, rock-liner interaction; IV, liner.

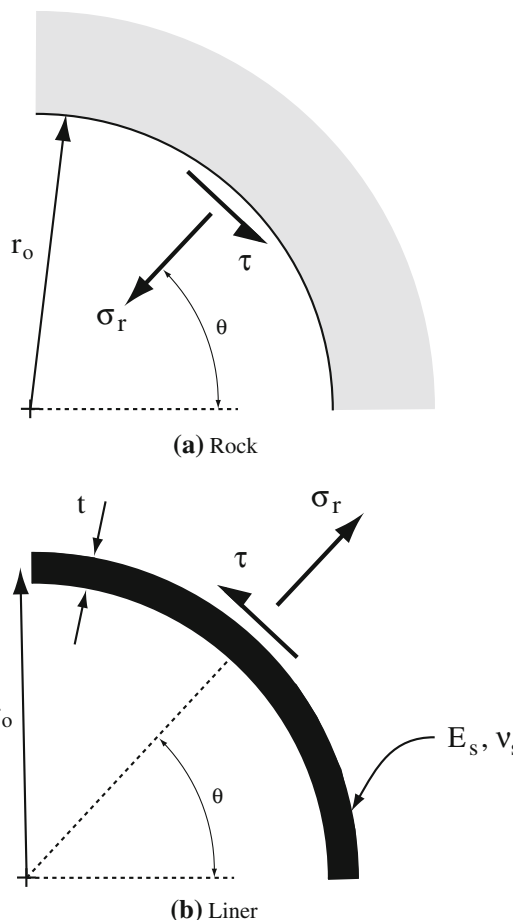


Fig. 3 Stresses at the Rock-liner interface

Problems I plus II give the solution of an opening in an infinite transversely anisotropic medium subjected to far-field stresses $\sigma_v, \sigma_h, \tau_{vh}$. This is so because the radial stresses and shear stresses applied to the excavation in problem II are those of the far-field, but with opposite sign. That is

$$\begin{aligned} \sigma_r^o &= -\frac{1}{2} (\sigma_v + \sigma_h) + \frac{1}{2} (\sigma_v - \sigma_h) \cos 2\theta - \tau_{vh} \sin 2\theta \\ \tau^o &= -\frac{1}{2} (\sigma_v - \sigma_h) \sin 2\theta - \tau_{vh} \cos 2\theta \end{aligned} \tag{16}$$

Problem III incorporates the radial and shear stresses that will be induced because of the liner. These are the stresses, with opposite sign, that are applied to the liner, as shown in Fig. 4e. Due to the symmetry of the problem and the loading, the stresses due to rock-liner interaction are of the form

$$\begin{aligned} \Delta \sigma_r &= \sigma_o + \sum_{n=2,4,6}^{\infty} \sigma_n^a \cos n\theta + \sum_{n=2,4,6}^{\infty} \sigma_n^b \sin n\theta \\ \Delta \tau &= \sum_{n=2,4,6}^{\infty} \tau_n^a \sin n\theta + \sum_{n=2,4,6}^{\infty} \tau_n^b \cos n\theta \end{aligned} \tag{17}$$

where $\sigma_o, \sigma_n^a, \sigma_n^b, \tau_n^a$ and τ_n^b are constants that depend on the boundary conditions. The constants are obtained by imposing compatibility of displacements between the rock and the liner. This is given by

$$\begin{aligned} U_x^{IV} &= U_x^{II} + U_x^{III} \\ U_y^{IV} &= U_y^{II} + U_y^{III} \end{aligned} \tag{18}$$

In Eq. 18 the conditions must be imposed term-by-term, i.e., for the constant term and for the terms with $\sin \theta, \cos \theta, \sin 2\theta, \cos 2\theta$, and so forth. The result is a system of equations that, when solved, provides the values of the constants $\sigma_o, \sigma_n^a, \sigma_n^b, \tau_n^a$, and τ_n^b . Note that the constants σ_o, σ_n^a , and τ_n^a depend on the far-field stresses σ_v and σ_h , while the constants σ_n^b and τ_n^b depend on the far-field shear stress τ_{vh} . It is implicitly stated in Eq. 18 that tunnel excavation and liner installation occur simultaneously. In other words, three-dimensional effects at the face of the tunnel are neglected. This means that all deformations that occur in the rock ahead of the face of the tunnel are not considered. Thus, the final deformations in the rock computed with the equations obtained are smaller than those from a three-dimensional analysis. As a result, and because of the elastic response of both the rock and the liner, the stresses of the liner are larger than those obtained when face effects are included.

The stresses in the rock are given by the sum of the stresses of Problems I, II, and III. Displacements are given by the sum of the displacements of problems II and III. This is so because problem I corresponds to the initial

conditions, and hence displacements have occurred before the liner is placed. Stresses and displacements of the liner are the result of problem IV.

Displacements of the rock medium are obtained by integration of strains, i.e., by integration of Eq. 5. They are given by

$$\begin{aligned} U_x &= 2Re[(\alpha_1\mu_1^2 - \alpha_2)\phi_1(z_1) + (\alpha_1\mu_2^2 - \alpha_2)\phi_2(z_2)] \\ U_y &= 2Re\left[\left(-\alpha_2\mu_1 + \frac{\alpha_3}{\mu_1}\right)\phi_1(z_1) + \left(-\alpha_2\mu_2 + \frac{\alpha_3}{\mu_2}\right)\phi_2(z_2)\right] \end{aligned} \tag{19}$$

Displacements and stresses of the liner are related by (Flügge 1966)

$$\begin{aligned} \frac{d^2 U_\theta^s}{d\theta^2} + \frac{dU_r^s}{d\theta} &= -\frac{(1 - \nu_s^2)}{E_s A_s} r_o^2 \tau^s \\ \frac{dU_\theta^s}{d\theta} + U_r^s + \frac{I_s}{r_o^2 A_s} \left(\frac{d^4 U_r^s}{d\theta^4} + 2 \frac{d^2 U_r^s}{d\theta^2} + U_r^s \right) &= \frac{(1 - \nu_s^2)}{E_s A_s} r_o^2 \sigma_r^s \end{aligned} \tag{20}$$

where U_r^s and U_θ^s are the radial and tangential displacements of the liner, σ_r^s and τ^s are the radial and shear stresses applied to the liner. In this case, $U_r^s = U_r^{IV}, U_\theta^s = U_\theta^{IV}$, and $\sigma_r^s = \Delta\sigma_r$, and $\tau^s = \Delta\tau$ which are given in Eq. 17. This is so because of the assumption of no slip and no detachment at the contact between the rock and the liner. A_s and I_s are the cross-sectional area and moment of inertia of the liner, respectively, E_s and ν_s are the Young's modulus and Poisson's ratio of the liner, and r_o is the radius of the tunnel (see Fig. 3b).

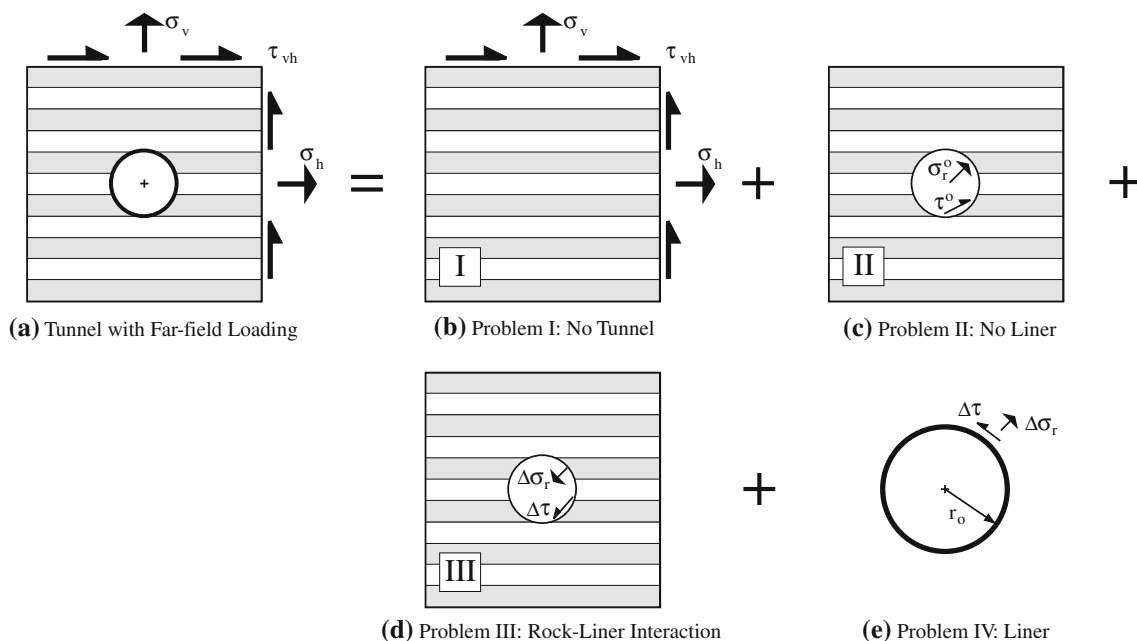


Fig. 4 Deep tunnel in dry rock

The thrust load T^s and moment distribution M^s in the liner are found from the following expressions

$$r_o \frac{dT^s}{d\theta} - \frac{dM^s}{d\theta} = -r_o^2 \tau^s \tag{21}$$

$$r_o T^s + \frac{d^2 M^s}{d\theta^2} = r_o^2 \sigma_r^s$$

Stresses and displacements of Problem I are

$$\begin{aligned} \sigma_x &= \sigma_h \\ \sigma_y &= \sigma_v \\ \tau_{xy} &= \tau_{vh} \\ U_x &= U_y = 0 \end{aligned} \tag{22}$$

The stress functions for Problems II and III are Problem II:

$$\begin{aligned} \phi_1 &= -\frac{1}{2} \frac{r_o}{\mu_1 - \mu_2} [(1 + \mu_2)\tau_{vh} + (\mu_2\sigma_v - \sigma_h)i] \frac{i}{\zeta_1} \\ \phi_2 &= \frac{1}{2} \frac{r_o}{\mu_1 - \mu_2} [(1 + \mu_1)\tau_{vh} + (\mu_1\sigma_v - \sigma_h)i] \frac{i}{\zeta_2} \end{aligned} \tag{23}$$

The solution of Problem II has been obtained by others (e.g., Lekhnitskii 1963; Hefny and Lo 1999) and is included here for completeness.

Problem III:

$$\begin{aligned} \phi_1 &= \frac{1}{4} \frac{r_o}{\mu_1 - \mu_2} \left\{ [2(1 - \mu_2)\sigma_o + (\sigma_2^a - \tau_2^a)(1 + \mu_2) + (\sigma_2^b + \tau_2^b)(1 + \mu_2)i] \frac{1}{\zeta_1} \right. \\ &\quad \left. + \sum_{n=3,5,7}^{\infty} \frac{1}{n} [(1 - \mu_2)(\sigma_{n-1}^a + \tau_{n-1}^a + i\sigma_{n-1}^b - i\tau_{n-1}^b) + (1 + \mu_2)(\sigma_{n+1}^a - \tau_{n+1}^a + i\sigma_{n+1}^b + i\tau_{n+1}^b)] \frac{1}{\zeta_1^n} \right\} \\ \phi_2 &= -\frac{1}{4} \frac{r_o}{\mu_1 - \mu_2} \left\{ [2(1 - \mu_1)\sigma_o + (\sigma_2^a - \tau_2^a)(1 + \mu_1) + (\sigma_2^b + \tau_2^b)(1 + \mu_1)i] \frac{1}{\zeta_2} \right. \\ &\quad \left. + \sum_{n=3,5,7}^{\infty} \frac{1}{n} [(1 - \mu_1)(\sigma_{n-1}^a + \tau_{n-1}^a + i\sigma_{n-1}^b - i\tau_{n-1}^b) + (1 + \mu_1)(\sigma_{n+1}^a - \tau_{n+1}^a + i\sigma_{n+1}^b + i\tau_{n+1}^b)] \frac{1}{\zeta_2^n} \right\} \end{aligned} \tag{24}$$

where μ_1 and μ_2 in Eqs. 23 and 24 are the modulus of the complex roots, i.e., they are real numbers.

Displacements are obtained from Eq. 19 and stresses from Eq. 11 after taking the derivatives of the stress functions in Eqs. 23 and 24. The derivatives of the functions are included in Appendix I. The displacements at the excavation, i.e., at $r = r_o$, are needed in Eq. 18 to obtain the constants σ_o , σ_n^a , σ_n^b , τ_n^a , and τ_n^b . Their expressions are included in Appendix II.

Problem IV:

The stresses acting on the liner are given by Eq. 17. The displacements of the liner are obtained after integration of Eq. 20 and are included in Appendix II. The thrust force and moment of the liner are obtained from Eq. 21 and are

$$\begin{aligned} T^s &= \sigma_o r_o - \sum_{n=2,4,6}^{\infty} \left\{ \left[\frac{\sigma_n^a - n\tau_n^a}{n^2 - 1} \right] r_o \cos n\theta \right. \\ &\quad \left. + \left[\frac{n\sigma_n^b + \tau_n^b}{n(n^2 - 1)} + \frac{\tau_n^b}{n} \right] r_o \sin n\theta \right\} \\ M^s &= - \sum_{n=2,4,6}^{\infty} \left\{ \left[\frac{n\sigma_n^a - \tau_n^a}{n(n^2 - 1)} \right] r_o^2 \cos n\theta + \left[\frac{n\sigma_n^b + \tau_n^b}{n(n^2 - 1)} \right] r_o^2 \sin n\theta \right\} \end{aligned} \tag{25}$$

Results from the analytical solution are compared with those from the Finite Element Method code ABAQUS (ABAQUS 2009). The following case is analyzed: deep tunnel with circular cross section with radius $r_o = 2$ m; rock properties, $E_x = 7,800$ MPa, $E_y = 2,400$ MPa, $\nu_{xy} = 0.07$, $\nu_{xz} = 0.22$, $\nu_{yz} = 0.02$, $G_{xy} = 830$ MPa (the properties are those of the bedded sedimentary Waichecheng series, from Tonon and Amadei 2002); liner properties, $E_s = 20,000$ MPa, $\nu_s = 0.3$, $t = 0.1$ m; compressive far-field loading with $\sigma_v^{ff} = -1$ MPa, $\sigma_h^{ff} = -0.5$ MPa with the bedding parallel to the tunnel axis and dipping 45° (i.e.,

angle β as defined in Fig. 2a is 45°), which results in $\sigma_v = \sigma_h = -0.75$ MPa and $\tau_{vh} = -0.25$ MPa. Note that the tunnel would be at about 40 m deep, given a typical rock unit weight, which would yield a depth to radius ratio of 20; in this case the tunnel can be considered deep (Peck et al. 1972; Bobet 2003). The simulations in ABAQUS are done in two steps. In the first step, the initial stresses, i.e., the far-field stresses, are applied to the unperforated rock medium. ABAQUS has a feature that allows zeroing all displacements

while maintaining the initial stresses. This is necessary to ensure that the liner, when placed, does not have to accommodate the rock deformations due to the geostatic (i.e., initial) stresses. In the second step the elements corresponding to the tunnel excavation are deactivated and the liner elements are activated.

Figure 5 shows the comparison in terms of stresses $p = \frac{1}{2}(\sigma_1 + \sigma_3)$ and $q = \frac{1}{2}(\sigma_1 - \sigma_3)$ in the rock, with σ_1 and σ_3 being the major and minor principal stresses. Only one quarter of the medium is used for the comparison. There are two reasons for this: one, what is intended is to show that the results from the analytical solution are correct; two, the problem has symmetry even though the rock is anisotropic. The x - and y -axes are axes of symmetry

when the far-field loading is given by σ_v and σ_h only, i.e., no shear, and they are axes of anti-symmetry when only shear is applied. Figure 6 is a plot of the stresses and displacements of the liner obtained with the two methods (see Fig. 3 for a definition of the angle θ). The comparisons are acceptable, and so the analytical solution is correct. Note that the radial stresses applied to the liner are compressive, which indicates that there is no detachment of the liner from the rock. If the radial stresses were tensile, the solution would not be valid, as it would violate the assumption of tied contact.

Figure 7 illustrates the effects of the orientation of the axes of elastic symmetry with respect to the direction of loading, i.e., effects of angle β (see Fig. 2). Using the

Fig. 5 Comparison between FEM and analytical solution for dry ground, with $r_o = 2$ m, $E_x = 7,800$ MPa, $E_y = 2,400$ MPa, $\nu_{xy} = 0.07$, $\nu_{xz} = 0.22$, $\nu_{yz} = 0.02$, $G_{xy} = 830$ MPa, $E_s = 20,000$ MPa, $\nu_s = 0.3$, $t = 0.1$ m, $\sigma_v^{ff} = -1$ MPa, $\sigma_h^{ff} = -0.5$ MPa, $\beta = 45^\circ$; $p = 1/2(\sigma_1 + \sigma_3)$, $q = 1/2(\sigma_1 - \sigma_3)$

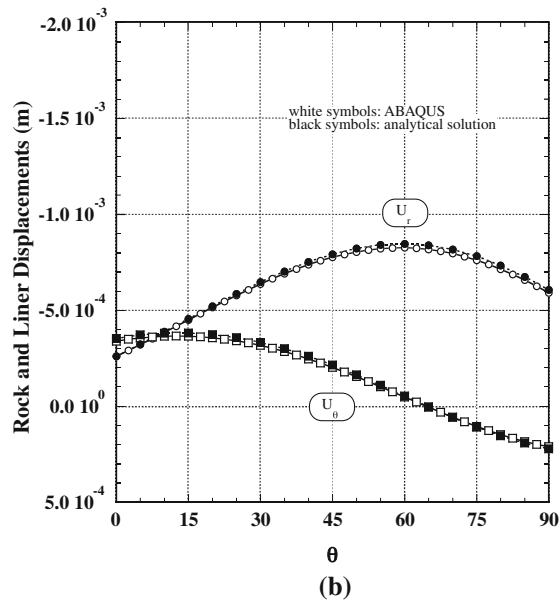
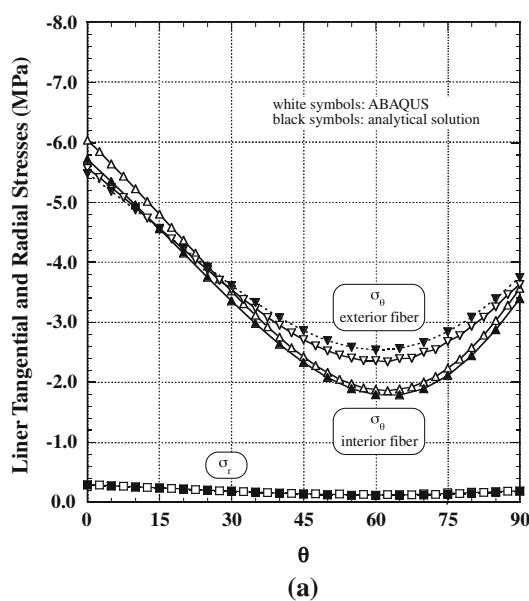
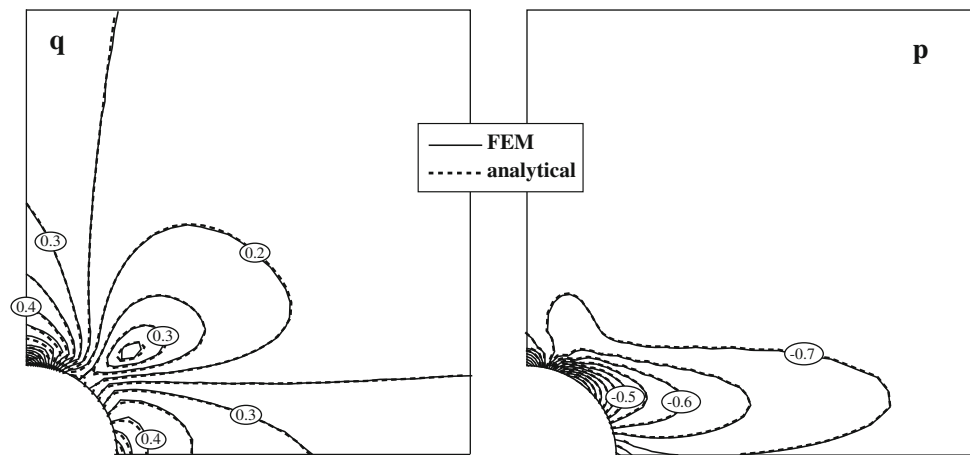


Fig. 6 Liner stresses and displacements. Comparison between ABAQUS and Analytical Solution, $r_o = 2$ m, $E_x = 7,800$ MPa, $E_y = 2,400$ MPa, $\nu_{xy} = 0.07$, $\nu_{xz} = 0.22$, $\nu_{yz} = 0.02$, $G_{xy} = 830$ MPa,

$E_s = 20,000$ MPa, $\nu_s = 0.3$, $t = 0.1$ m, $\sigma_v^{ff} = -1$ MPa, $\sigma_h^{ff} = -0.5$ MPa, $\beta = 45^\circ$

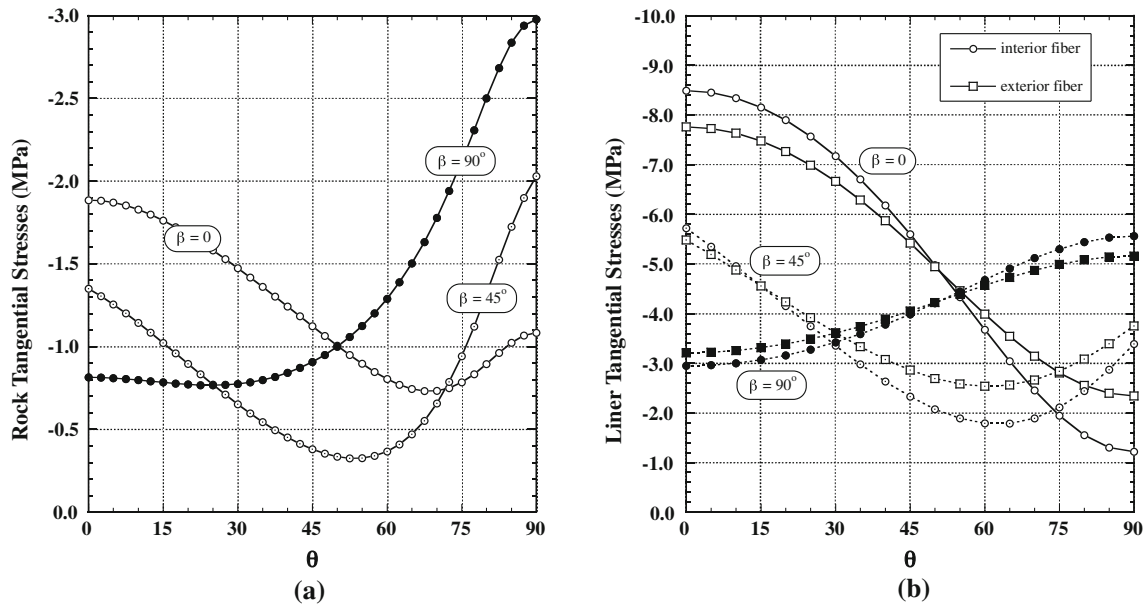


Fig. 7 Rock and liner stresses. Effect of angle of isotropic symmetry β . $r_o = 2\text{ m}$, $E_x = 7,800\text{ MPa}$, $E_y = 2,400\text{ MPa}$, $\nu_{xy} = 0.07$, $\nu_{xz} = 0.22$, $\nu_{yz} = 0.02$, $G_{xy} = 830\text{ MPa}$, $E_s = 20,000\text{ Mpa}$, $\nu_s = 0.3$, $t = 0.1\text{ m}$, $\sigma_v^{ff} = -1\text{ MPa}$, $\sigma_h^{ff} = -0.5\text{ MPa}$

analytical solution, three cases are considered, $\beta = 0^\circ$, 45° , 90° . In the first case ($\beta = 0^\circ$) the y -axis coincides with the vertical far-field stress, i.e. horizontal bedding; in the third case ($\beta = 90^\circ$), the y -axis is horizontal and is along the direction of the horizontal far-field stress, i.e., vertical bedding; in the second case, the far-field stresses make an angle of 45° with respect to the y -axis, i.e., the bedding dip is 45° . Tunnel geometry, rock, and liner properties are the same as those used for the calculations presented in Figs. 5 and 6. Figure 7a is a plot of the tangential stresses of the rock in contact with the liner, i.e., at $r = r_o$, and Fig. 7b is a plot of the stresses in the liner. Radial stresses in all cases are compressive (not shown in the figures), which indicates that there is no detachment of the liner from the rock. It is interesting to note in Fig. 7b that for $\beta = 0^\circ$, 90° the maximum and minimum liner stresses occur at $\theta = 0^\circ$, 90° . This is expected given Eq. 17, where for $\tau_{vh} = 0$, i.e., $\beta = 0^\circ$, 90° , the terms σ_n^b and τ_n^b are zero, and so the stress functions attain their maxima or minima when $\theta = 0$ or $\pi/2$. For the third case analyzed in Fig. 7, $\beta = 45^\circ$, where none of the far-field stresses are zero, a minimum occurs at a location other than $\theta = 0, \pi/2, \pi/4$ (note that the maxima and minima at $\theta = \pi/4$ occur when $\sigma_v = \sigma_h = 0$ because the terms σ_o , σ_n^a and σ_n^b are zero). Figure 7b shows that the most non-uniform liner stresses occur for $\beta = 0^\circ$. This is the case where the largest far-field stress, σ_v , is aligned with the axis of elastic symmetry (y -axis) where the stiffness is the smallest. Because of the non-uniform far-field stress, larger radial deformations and

smaller radial stresses, i.e., larger unloading, occur at the crown than at the springline. This mechanism is augmented by the lower stiffness in the vertical direction than in the horizontal direction. For $\beta = 90^\circ$ the larger stiffness along the vertical direction allows the rock to deform less and thus take more load. This is shown in Figs. 7a, b as larger tangential stresses in the rock and smaller tangential stresses in the liner. The third case, $\beta = 45^\circ$, can be considered as intermediate between the two.

The response of a lined tunnel in transversely anisotropic rock can be further explored by comparing the distortion that occurs in an unlined tunnel with isotropic material and with transversely anisotropic material. Both cases are analyzed with uniform far-field loading, $\sigma_v^{ff} = \sigma_h^{ff} = \sigma_o^{ff}$. For the case of isotropic rock, the radial displacements at the tunnel perimeter are given by the following expression (e.g. Einstein and Schwartz 1979)

$$U_r = \frac{1 + \nu}{E} \sigma_o^{ff} r_o \tag{26a}$$

For the case of transversely anisotropic rock (from Eq. 38)

$$U_r = \frac{1}{2} \{ [\mu_1 + \mu_2 + (\mu_1 + \mu_2 - 2) \mu_1 \mu_2] \alpha_1 + 2\alpha_2 - (\mu_1 + \mu_2)(\mu_1 \mu_2 - 1) \alpha_1 \cos 2\theta \} \sigma_o^{ff} r_o \tag{26b}$$

In the first case, isotropic rock, the radial displacements are constant, while in the second case they change with the angle θ , and so even with constant pressures, the displacements are

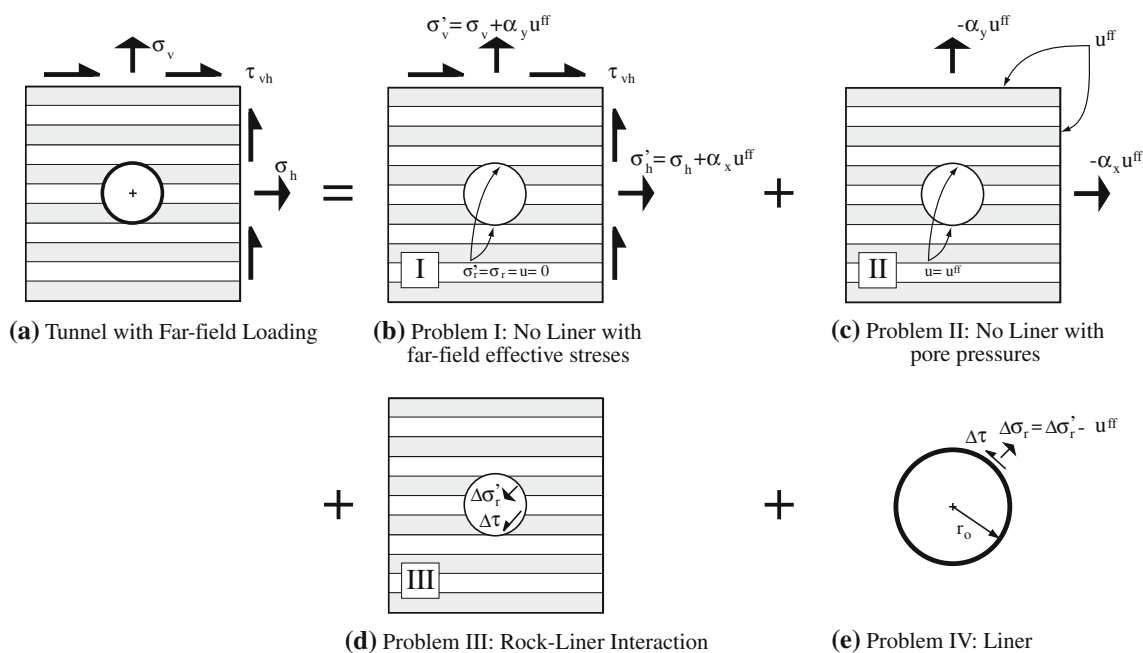


Fig. 8 Deep tunnel below the water table. Effective stress decomposition

not uniform. This indicates that the stresses in the liner, since they are related to the displacements of the unsupported tunnel, are also not uniform, and so bending of the liner will occur in anisotropic rock even if the far-field applied stresses are uniform.

3.3 Below the Groundwater Table

Tunnels below the water table and with impermeable lining are subjected to a uniform pore pressure with magnitude u^{ff} , which is determined by the product of the unit weight of the pore fluid times the depth of the center of the tunnel. The liner is thus subjected to stresses that come from the rock (effective stresses) and those of the pore pressure. It is important to realize that the pore pressures may induce effective stresses in the rock, and thus contribute to deformations. This is so because, if the liner is compressible, it will deform towards the opening due to the pore pressures on the exterior of the liner, i.e., at the contact with the rock. Because the rock must remain attached to the liner, it must also move with the liner (note that it is assumed that the final radial stresses on the liner are compressive, i.e., no gap forms between the rock and the liner). Since deformations are only possible with effective stresses, then it follows that pore pressures may cause effective stresses.

It will be shown, however, that despite the fundamental differences that exist between a tunnel in dry rock and a tunnel below the water table, the end result is that stresses

in the liner, displacements of the liner and rock, and total stresses in the rock for a tunnel below the water table are the same as those of a tunnel excavated in dry ground, as long as the total far-field stresses are the same in both cases. This statement can be supported by computing separately the contributions of effective stresses and pore pressures. Figure 8a shows the tunnel with far-field total stresses σ_v , σ_h , and τ_{vh} . The problem is decomposed into four other problems. Problem I, Fig. 8b, corresponds to the tunnel without the liner and subjected to effective stresses in the far-field; since there is no liner, the total and effective radial stresses and shear stresses at the opening are zero. Note that the problem is defined completely in terms of effective stresses. Problem II, Fig. 8c, includes the contribution of the pore pressures. The figure describes a circular opening filled with water at a pressure u^{ff} with far-field pore pressures also u^{ff} . Note that total far-field vertical and horizontal stresses with magnitude $-\alpha_y u^{ff}$ and $-\alpha_x u^{ff}$, respectively, are applied; they are necessary because the sum of the total far-field stresses in Problems I and II must add up to those in Fig. 8a. Problem III, as denoted in Fig. 8d, represents the interaction between the rock and the liner, i.e., the stresses induced in the rock because of the presence of the liner as the deformations of the rock must be those of the liner. Finally, Problem IV in Fig. 8e represents the liner subjected to the stresses from the rock. At the interface between the liner and the rock, the total stresses acting on the liner must be the same as those on the rock, the pore

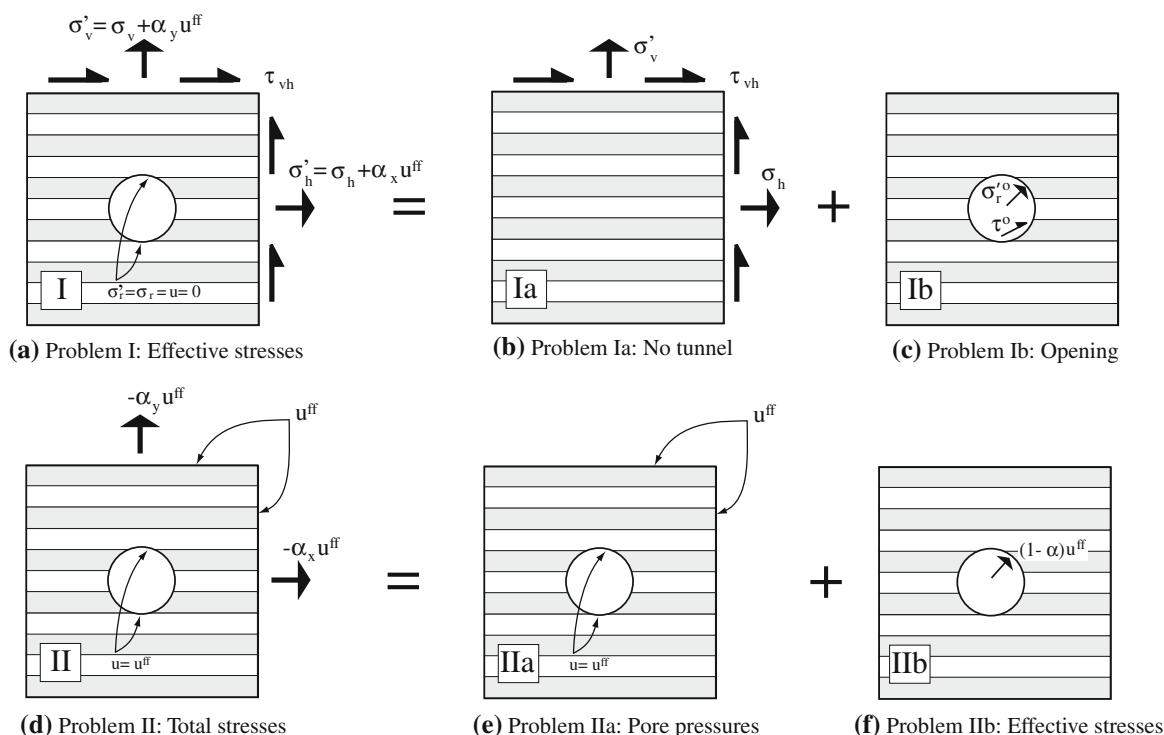


Fig. 9 Stress decomposition of Problems I and II (Fig. 8)

pressures at the contact are equal to the ambient pore pressures u^{ff} and the displacements of the liner and of the rock are the same. Problem I can be further decomposed into Problems Ia and Ib; see Figs. 9a–c. Problem Ia represents the unperforated ground subjected to far-field effective stresses $\sigma'_v = \sigma_v + \alpha_y u^{ff}$ and $\sigma'_h = \sigma_h + \alpha_x u^{ff}$. Problem Ib in Fig. 9c includes the effective stresses that need to be placed at the perimeter of the opening such that Problems Ia and Ib are equal to problem I; that is the stresses in Ib are the same with opposite sign as those of Problem Ia at the location of the perimeter of the opening. The stresses in Problem II (Fig. 8c, also repeated in Fig. 9d) are decomposed into pore pressures, problem IIa shown in Fig. 9e, and effective stresses, Problem IIb shown in Fig. 9f.

Figure 4 (dry ground or tunnel above the water table) represents the decomposition of a problem similar to that shown in Fig. 8 (tunnel below the water table). It can be shown that the decomposition used in Fig. 4, and thus the corresponding analytical solutions, is exactly the same as that of Fig. 8. This is done considering the following:

1. Problem I in Fig. 4 is exactly Problem Ia (Fig. 9b) plus Problem IIa (Fig. 9e).
2. Problem II in Fig. 4 is exactly Problem Ib (Fig. 9c) plus Problem IIb (Fig. 9f) except for the compressive

radial effective stresses with magnitude u^{ff} at the perimeter of the opening. Indeed, the radial stresses at the opening from Problems Ib and IIb are: $\sigma'_r + (1 - \alpha)u^{ff} = (\sigma'_r - \alpha u^{ff}) + u^{ff}$; the expression in parenthesis is the total stress σ'_r , which is that shown in Problem II in Fig. 4. The extra term u^{ff} is added to Problem III, Fig. 8d; see next point.

3. Problem III in Fig. 4 is exactly problem III in Fig. 8 with the addition of the compressive radial stresses u^{ff} discussed in the preceding point.
4. Problem IV in Fig. 4 is equal to Problem IV in Fig. 8.

Hence, the preceding statement that concludes that the total stresses and displacements in the rock and liner for a tunnel with impermeable liner can be obtained from the equations derived for a tunnel in dry rock is correct as long as total stresses are used as input in the calculations. In other words, Eqs. 23 and 24 and Eqs. 37–42 that were derived for dry rock are also valid for saturated rock below the water table.

Figure 10 shows a comparison between results obtained from the analytical solution and those from ABAQUS for a tunnel below the water table. The tunnel geometry and material properties are the same as those used in all the previous examples, except that the far-field stresses are as follows: $\sigma_v = -2.0$ MPa, $\sigma_h = -1.5$ MPa,

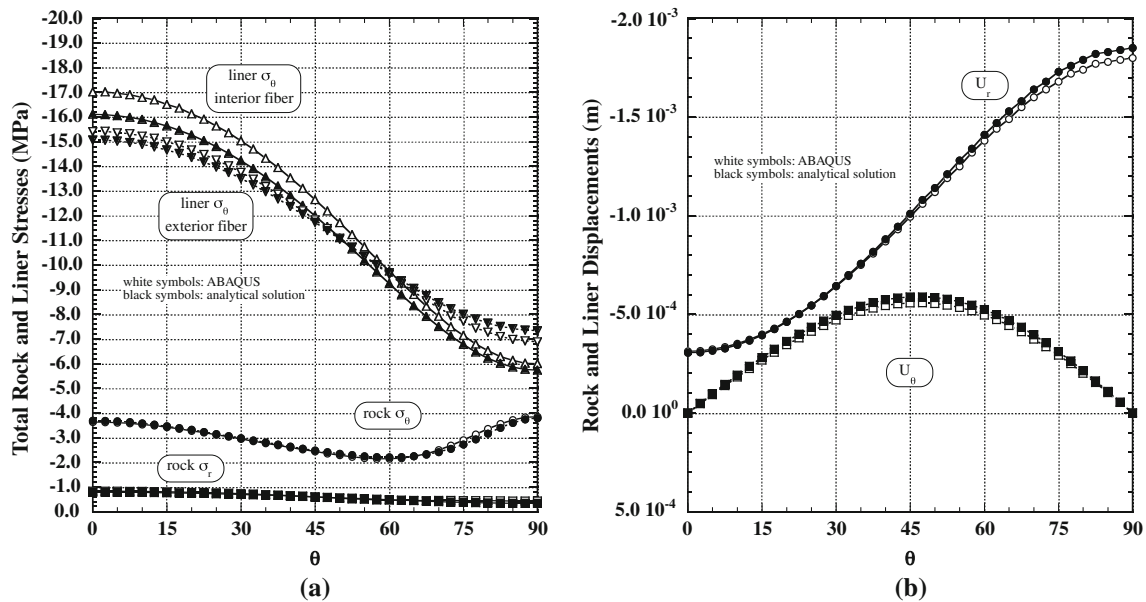


Fig. 10 Rock and liner stresses and liner displacements. Comparison between ABAQUS and analytical solution. Deep tunnel below water table. $r_o = 2$ m, $E_x = 7,800$ MPa, $E_y = 2,400$ MPa, $\nu_{xy} = 0.07$,

$\nu_{xz} = 0.22$, $\nu_{yz} = 0.02$, $G_{xy} = 830$ MPa, $\alpha_x = \alpha_y = 1$, $M \gg 1$, $E_s = 20,000$ MPa, $\nu_s = 0.3$, $t = 0.1$ m, $\sigma_v = -2$ MPa, $\sigma_h = -1.5$ MPa, $u^{ff} = 0.25$ MPa, $\beta = 0^\circ$

$\tau_{vh} = 0$, $\beta = 0^\circ$, $u^{ff} = 0.25$ MPa. The simulations in ABAQUS, similar to the case with dry rock, are done in two steps. In the first step, the far-field stresses are imposed with zero displacements. In the second step the elements corresponding to the tunnel opening are deactivated and those of the liner are activated. Since ABAQUS can only model materials following Terzaghi’s principle of effective stresses, the values of the Biot’s parameters α_x and α_y in the analytical solution are $\alpha_x = \alpha_y = 1$, and the Biot’s modulus M is given a very large value. Figure 10a shows total tangential stresses in the liner and total tangential and radial stresses in the rock adjacent to the liner, while Fig. 10b shows radial and tangential displacements. The effective radial stresses at the rock-liner contact are compressive, which satisfies the assumption of a tied contact. The figures show that the results are acceptable, with differences smaller than 2%, except perhaps for the tangential stresses in the interior fiber of the liner where the differences are up to 5%. The comparisons not only show that the analytical solution provides accurate results, but also that stresses and displacements do not change if there is water pressure as long as total stresses are used for the calculations. Note that the trends of rock and liner stresses shown in Fig. 10 are similar to those in Fig. 7 for $\beta = 0^\circ$. There are expected differences in magnitude since the total far-field stresses are not the same, but the overall shape of the tangential stresses in the liner and in the rock are similar.

4 Tunnel in Saturated Rock Subjected to Undrained Shear

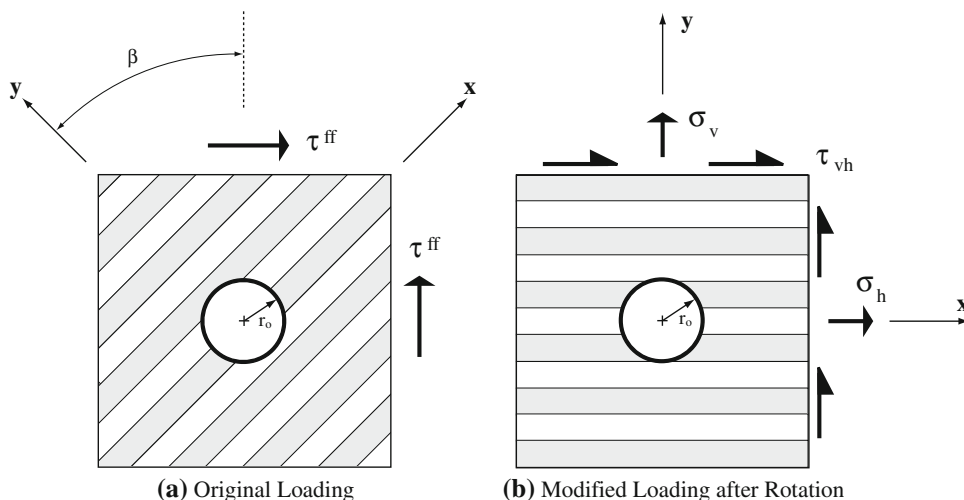
A mode of loading that is of interest is that of far-field shear. This is because seismic loading of tunnels placed far from the seismic source can be approximated by a quasi-static analysis, where the magnitude of the shear stress or shear strain induced by the earthquake in the free-field (i.e., without the tunnel) is applied to the far-field (Wang 1993). See Fig. 11a. The quasi-static analysis is acceptable when the wavelength of peak velocities induced by the earthquake is at least eight times larger than the width of the opening (Hendron and Fernández 1983; Merritt et al. 1985; and Monsees and Merritt 1988).

The direction of the far-field shear loading is oriented at angle β with the axis of elastic symmetry, as shown in Fig. 11a. The far-field shear loading, τ^{ff} , after a rotation of angle β , can be expressed in terms of σ_v , σ_h and τ_{vh} as

$$\begin{aligned} \sigma_v &= -\tau^{ff} \sin 2\beta \\ \sigma_h &= \tau^{ff} \sin 2\beta \\ \tau_{vh} &= \tau^{ff} \cos 2\beta \end{aligned} \tag{27}$$

The solution of the problem requires solving Eq. 9. Because of rapid loading, excess pore pressures will be generated such that no change of fluid volume in the rock occurs, i.e., undrained conditions apply. This requires that $\Delta\zeta = 0$, and so the excess pore pressures can be found, from Eqs. 7 and 5, as

Fig. 11 Deep tunnel with quasi-static seismic loading



$$u = -M(\alpha_x \epsilon_x + \alpha_y \epsilon_y) = -\frac{1}{\beta_3}(\beta_1 \sigma_x + \beta_2 \sigma_y) \tag{28}$$

$$\beta_3 = \frac{1}{M} + \alpha_x \beta_1 + \alpha_y \beta_2$$

Strains are obtained from Eqs. 28 and 5 and are

$$\begin{aligned} \epsilon_x &= \left(\alpha_1 - \frac{\beta_1^2}{\beta_3}\right)\sigma_x - \left(\alpha_2 + \frac{\beta_1\beta_2}{\beta_3}\right)\sigma_y \\ \epsilon_y &= -\left(\alpha_2 + \frac{\beta_1\beta_2}{\beta_3}\right)\sigma_x + \left(\alpha_3 - \frac{\beta_2^2}{\beta_3}\right)\sigma_y \\ \gamma &= \frac{\tau_{xy}}{G_{xy}} \end{aligned} \tag{29}$$

The compatibility equation now takes the form

$$\begin{aligned} \left(\alpha_1 - \frac{\beta_1^2}{\beta_3}\right)\frac{\partial^4 F}{\partial y^4} + \left(\alpha_3 - \frac{\beta_2^2}{\beta_3}\right)\frac{\partial^4 F}{\partial x^4} \\ + \left(\frac{1}{G_{xy}} - 2\alpha_2 - 2\frac{\beta_1\beta_2}{\beta_3}\right)\frac{\partial^4 F}{\partial x^2 \partial y^2} = 0 \end{aligned} \tag{30}$$

which can be solved following a technique similar to that used for the case of a tunnel in dry rock. Eq. 11 for stresses, with $F_o = 0$, and Eq. 14 for the stress functions, are still valid. The complex numbers μ_1 and μ_2 are the roots of the equation

$$\begin{aligned} \left(\alpha_1 - \frac{\beta_1^2}{\beta_3}\right)\mu_k^4 + \left(\frac{1}{G_{xy}} - 2\alpha_2 - 2\frac{\beta_1\beta_2}{\beta_3}\right)\mu_k^2 \\ + \left(\alpha_3 - \frac{\beta_2^2}{\beta_3}\right) = 0 \end{aligned} \tag{31}$$

As with the case of dry rock, it can be shown that the roots of Eq. 31 are pure imaginary numbers. Given Eq. 31, the following applies

$$\begin{aligned} \mu_1^2 + \mu_2^2 &= -\frac{\left(\frac{1}{G_{xy}} - 2\alpha_2 - 2\frac{\beta_1\beta_2}{\beta_3}\right)}{\left(\alpha_1 - \frac{\beta_1^2}{\beta_3}\right)} \\ \mu_1^2 \mu_2^2 &= \frac{\left(\alpha_3 - \frac{\beta_2^2}{\beta_3}\right)}{\left(\alpha_1 - \frac{\beta_1^2}{\beta_3}\right)} > 0, \text{ and so} \\ \mu_1^2 + \mu_2^2 - 2\mu_1\mu_2 &= (\mu_1 - \mu_2)^2 = \frac{1}{\left(\alpha_1 - \frac{\beta_1^2}{\beta_3}\right)} \\ \left[-\frac{1}{G_{xy}} + 2\left(\alpha_2 + \frac{\beta_1\beta_2}{\beta_3}\right) - 2\sqrt{\left(\alpha_3 - \frac{\beta_2^2}{\beta_3}\right)\left(\alpha_1 - \frac{\beta_1^2}{\beta_3}\right)}\right] < 0 \end{aligned} \tag{32}$$

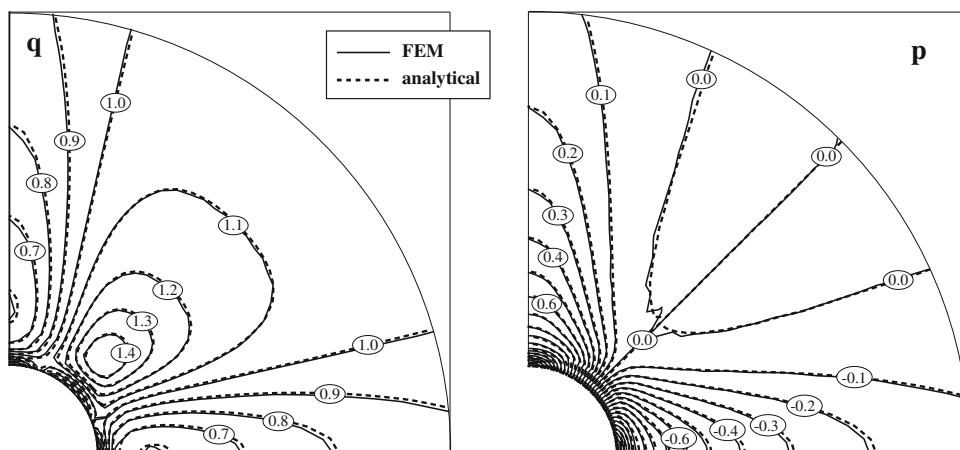
Note that $(\mu_1\mu_2) > 0$, as indicated in the second expression in Eq. 32 because both the numerator and denominator must be positive given the definition of strains in Eq. 29. Also, the compliance matrix must be positive definite, and so $(\alpha_3 - \beta_2^2/\beta_3)(\alpha_1 - \beta_1^2/\beta_3) > (\alpha_2 + \beta_1\beta_2/\beta_3)^2$. Hence $(\mu_1 - \mu_2)$ is an imaginary number. Following the same reasoning as before, the roots must be pure imaginary numbers.

The solution of the problem can be found in a manner analogous to what was done for the problem of a tunnel in dry rock. It can be decomposed into the same four problems shown in Fig. 4. Compatibility of displacements due to the four problems requires

$$\begin{aligned} U_x^{IV} &= U_x^I + U_x^{II} + U_x^{III} \\ U_y^{IV} &= U_y^I + U_y^{II} + U_y^{III} \end{aligned} \tag{33}$$

Note that, similar to the previous problems analyzed, it is assumed that the liner-rock interface is a tied contact. However, the assumption that no tension may be produced

Fig. 12 Comparison between FEM and analytical solution for undrained loading, with $r_o = 2$ m, $E_x = 7,800$ MPa, $E_y = 2,400$ MPa, $\nu_{xy} = 0.07$, $\nu_{xz} = 0.22$, $\nu_{yz} = 0.02$, $G = 830$ MPa, $E_s = 20,000$ MPa, $\nu_s = 0.3$, $t = 0.1$ m, $\alpha_x = \alpha_y = 1.0$, $M \gg 1$, $\tau^{ff} = 1$ MPa, $\beta = 45^\circ$; $p = 1/2 (\sigma_1 + \sigma_3)$, $q = 1/2 (\sigma_1 - \sigma_3)$



at the contact due to the far-field shear can be relaxed as long as the addition of the radial stresses due to the shear and the pre-existing radial stresses, e.g., from construction, do not result in tension.

Displacements are obtained from the integration of strains from Eq. 29 and are, in terms of the stress functions

$$\begin{aligned}
 U_x &= 2Re \left\{ \left[\left(\alpha_1 - \frac{\beta_1^2}{\beta_3} \right) \mu_1^2 - \left(\alpha_2 + \frac{\beta_1 \beta_2}{\beta_3} \right) \right] \phi_1(z_1) + \left[\left(\alpha_1 - \frac{\beta_1^2}{\beta_3} \right) \mu_2^2 - \left(\alpha_2 + \frac{\beta_1 \beta_2}{\beta_3} \right) \right] \phi_2(z_2) \right\} \\
 U_y &= 2Re \left\{ \left[- \left(\alpha_2 + \frac{\beta_1 \beta_2}{\beta_3} \right) \mu_1 + \left(\alpha_3 - \frac{\beta_2^2}{\beta_3} \right) \frac{1}{\mu_1} \right] \phi_1(z_1) + \left[- \left(\alpha_2 + \frac{\beta_1 \beta_2}{\beta_3} \right) \mu_2 + \left(\alpha_3 - \frac{\beta_2^2}{\beta_3} \right) \frac{1}{\mu_2} \right] \phi_2(z_2) \right\}
 \end{aligned}
 \tag{34}$$

Note the similarity between Eqs. 34 and 19. Both sets of equations have the same structure, with differences only in terms of the factors of the functions $\phi(z)$. The expressions included in Appendix I and II are thus applicable to problems II, III, IV, and undrained conditions. Problem I has the solution

$$\begin{aligned}
 \sigma_x &= \sigma_h \\
 \sigma_y &= \sigma_v \\
 \tau_{xy} &= \tau_{vh} \\
 u &= -\frac{1}{\beta_3} (\beta_1 \sigma_h + \beta_2 \sigma_v) \\
 U_x &= \left[\left(\alpha_1 - \frac{\beta_1^2}{\beta_3} \right) \sigma_h - \left(\alpha_2 + \frac{\beta_1 \beta_2}{\beta_3} \right) \sigma_v \right] x + \frac{1}{2} \frac{\tau_{vh}}{G_{xy}} y \\
 U_y &= \left[- \left(\alpha_2 + \frac{\beta_1 \beta_2}{\beta_3} \right) \sigma_h + \left(\alpha_3 - \frac{\beta_2^2}{\beta_3} \right) \sigma_v \right] y + \frac{1}{2} \frac{\tau_{vh}}{G_{xy}} x
 \end{aligned}
 \tag{35}$$

The difference between Eqs. 35 and 22 for tunnels in dry rock or below the water table, e.g., problem I for dry ground, is that, in addition to the pore pressures, in Eq. 22

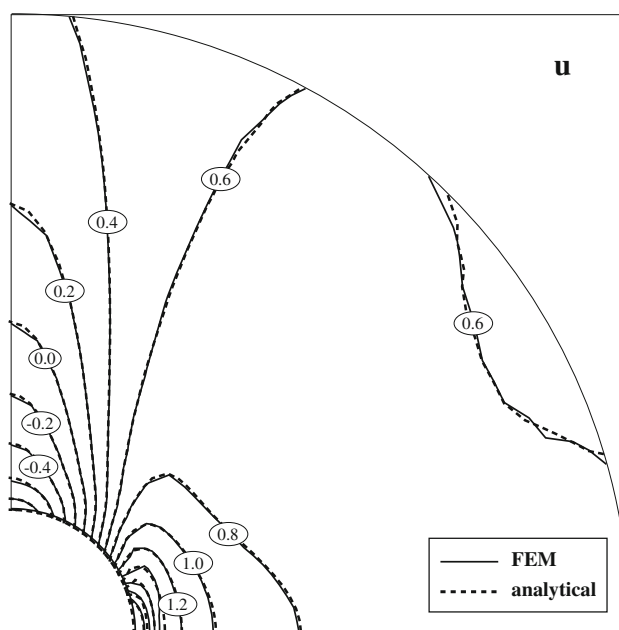


Fig. 13 Pore pressures from FEM and analytical solution for undrained loading $r_o = 2$ m, $E_x = 7,800$ MPa, $E_y = 2,400$ MPa, $\nu_{xy} = 0.07$, $\nu_{xz} = 0.22$, $\nu_{yz} = 0.02$, $G = 830$ MPa, $E_s = 20,000$ MPa, $\nu_s = 0.3$, $t = 0.1$ m, $\alpha_x = \alpha_y = 1.0$, $M \gg 1$, $\tau^{ff} = 1$ MPa, $\beta = 45^\circ$

the displacements are zero because they occurred before the tunnel is placed. In Eq. 35, however, the far-field stresses are applied while the tunnel is in place and so the displacements induced in the unperforated ground must be included. Consequently, the stresses in the liner and in the rock mass are the sum of tunnel construction and far-field shear. In the following, only stresses and displacements due to the far-field shear are discussed.

Figures 12, 13 and 14 present a comparison of the results obtained from the analytical solution and ABAQUS. Tunnel geometry, rock, and liner properties are the same as those considered in previous analyses, with the orientation

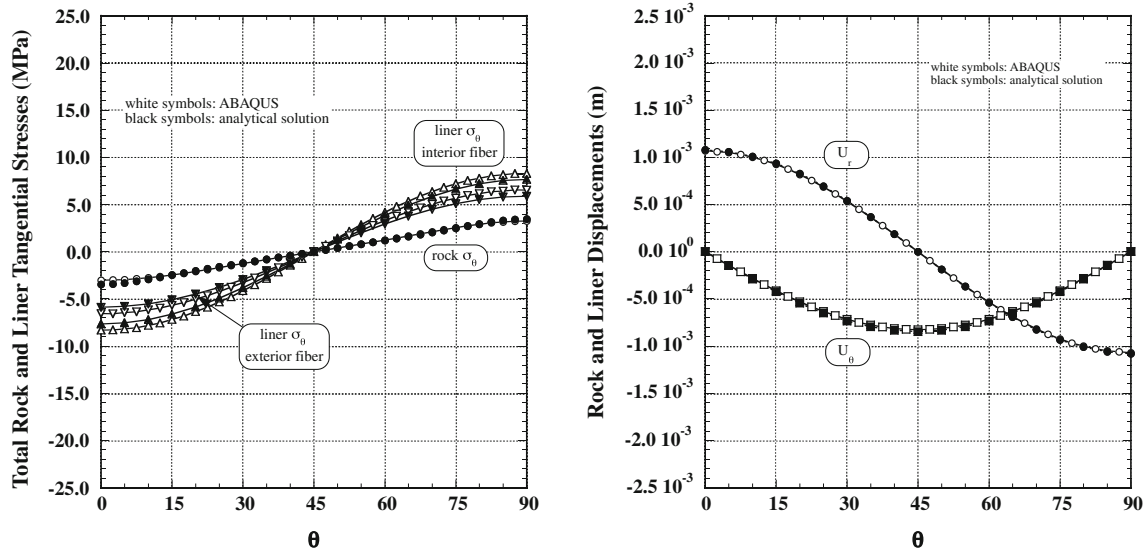
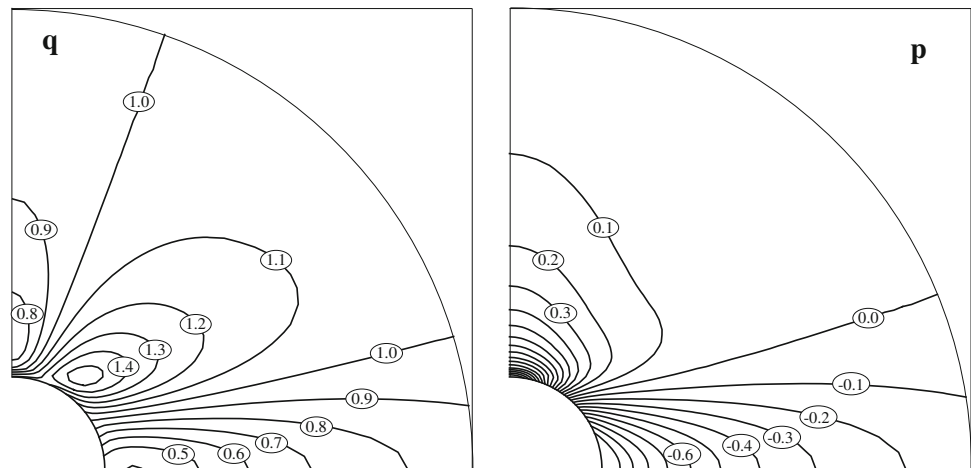


Fig. 14 Rock and liner stresses and liner displacements. Comparison between ABAQUS and analytical solution. Undrained analysis. $r_o = 2$ m, $E_x = 7,800$ MPa, $E_y = 2,400$ MPa, $\nu_{xy} = 0.07$, $\nu_{xz} =$

0.22 , $\nu_{yz} = 0.02$, $G_{xy} = 830$ MPa, $\alpha_x = \alpha_y = 1$, $M \gg 1$, $E_s = 20,000$ MPa, $\nu_s = 0.3$, $t = 0.1$ m, $\tau^{ff} = 1$ MPa, $\beta = 45^\circ$

Fig. 15 Shear loading, with dry rock and $r_o = 2$ m, $E_x = 7,800$ MPa, $E_y = 2,400$ MPa, $\nu_{xy} = 0.07$, $\nu_{xz} = 0.22$, $\nu_{yz} = 0.02$, $G = 830$ MPa, $E_s = 20,000$ MPa, $\nu_s = 0.3$, $t = 0.1$ m, $\tau^{ff} = 1$ MPa, $\beta = 45^\circ$; $p = 1/2(\sigma_1 + \sigma_3)$, $q = 1/2(\sigma_1 - \sigma_3)$



of the axes of elastic isotropy with respect to the far-field loading given by $\beta = 45^\circ$. The far-field loading is given by a shear stress $\tau^{ff} = 1$ MPa, i.e., $\sigma_v = -\sigma_h = -1.0$ MPa and $\tau_{vh} = 0$ (note that tension is taken as positive). For the rock, the Biot's constants are $\alpha_x = \alpha_y = 1$, and the Biot's modulus $M \gg 1$. The calculations in ABAQUS are done in one step, where the liner elements are activated and the excavation elements are deactivated. Undrained conditions in ABAQUS are approximated by imposing a time step very small, so there is no time for excess pore pressure dissipation.

Figure 12 is a contour plot of stresses $p = 1/2(\sigma_1 + \sigma_3)$ and $q = 1/2(\sigma_1 - \sigma_3)$ in the rock, where σ_1 and

σ_3 are the major and minor total principal stresses, and Fig. 13 is a contour plot of the pore pressures, also in the rock. As one can see the comparisons are acceptable. It is important to mention that pore pressures are generated in response to volumetric changes in the rock, which are associated with the mean stress and the stiffness of the rock, and so there is no reason why the pore pressures should be symmetric. Figure 14 introduces plots of the total tangential stresses and radial and tangential displacements of the liner obtained both with ABAQUS and with the analytical solution. Again, the comparisons are acceptable. In general, the differences are within the 1–2% range, except for the liner stresses, where they can be up to 5–6%.

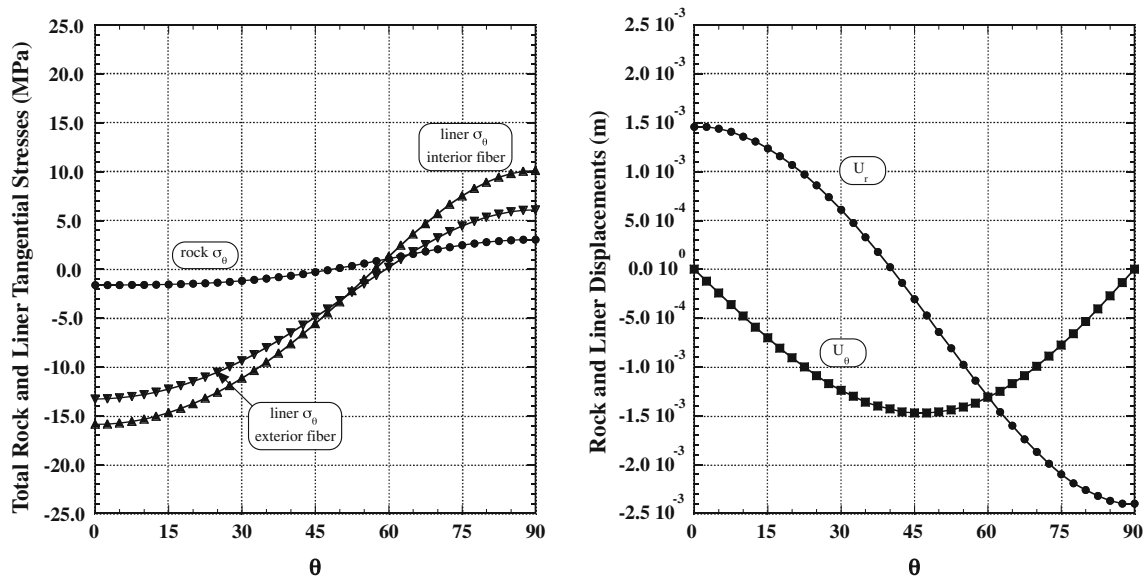


Fig. 16 Liner tangential stresses and displacements. Far-Field Shear. Dry Rock, $r_o = 2$ m, $E_x = 7,800$ MPa, $E_y = 2,400$ MPa, $\nu_{xy} = 0.07$, $\nu_{xz} = 0.22$, $\nu_{yz} = 0.02$, $G_{xy} = 830$ MPa, $E_s = 20,000$ MPa, $\nu_s = 0.3$, $t = 0.1$ m, $\tau^{ff} = 1$ MPa, $\beta = 45^\circ$

It is interesting to compare stresses and deformations that occur in a tunnel when excess pore pressures may occur and when they cannot (e.g., the rock is dry or the rock permeability is very high and so excess pore pressures dissipate before the end of the loading). Figures 15 and 16 are plots of the p - q stresses, tangential stresses, and displacements of the liner for the same tunnel as that used for the calculations shown in Figs. 12 to 14, but in dry ground; that is no excess pore pressures occur. The same formulation as for the undrained conditions can be used by taking the Biot's parameters $\alpha_x = \alpha_y = 0$ (note that this makes $\beta_1 = \beta_2 = 0$). A comparison between Figs. 12 (undrained, i.e., excess pore pressures) and 15 (dry, i.e., no excess pore pressures) indicates that the p and q stresses for the undrained scenario show symmetry with respect to an axis at 45° with the horizontal (the p stresses show anti-symmetry). For the dry ground there is a tendency of larger magnitudes of the p -stresses towards the horizontal axis. This is associated with the higher stiffness of the rock in the horizontal axis and lower stiffness in the vertical axis. It seems that, for undrained conditions, the excess pore pressures tend to reduce the non-uniformity of stresses in the rock, as the magnitude of the pore pressures is related to the tendency of the rock to deform. As one can see in Fig. 13, the magnitude of the pore pressures along the horizontal axis is larger than along the vertical axis, which tends to compensate the differences in p -stresses. In other words, if no excess pore pressures are produced (Fig. 15), the p -stresses are larger along the horizontal axis than along the vertical axis. If excess pore pressures occur, pore pressures

are larger at the locations where the p -stresses would be larger, and so the end result is an increase of uniformity around the tunnel. Further support of the “regularizing” effect of the pore pressures is found by comparing results between Figs. 14 and 16, which include tangential stresses in the liner and radial and tangential displacements of the liner. Figure 16 indicates that the magnitudes of stresses and displacements for the tunnel in dry rock are much larger than those of the tunnel with undrained conditions, and also that the differences between results at the springline and crown are larger. Note that for the tunnel with undrained conditions, the absolute magnitude of the results at the springline and the crown is very similar. In other words, excess pore pressures tend to mask the anisotropy of the rock and result in patterns similar to those that are produced in tunnels in isotropic rocks. The “regularizing” effect strongly depends on the magnitude of the Biot's parameters α_x and α_y . The smaller the parameters, the smaller the effect. Indeed, results for dry rock are obtained when $\alpha_x = \alpha_y = 0$, where no “regularizing” effect occurs.

5 Summary and Conclusions

The paper presents closed-form solutions for the stresses and displacements of a circular tunnel excavated in rock with transverse anisotropy. The tunnel may be placed above or below the water table and subjected to static or undrained seismic loading. The solutions are reached with the assumption of elastic response of the rock and the liner,

no-slip between the liner and the rock, impermeable liner, simultaneous excavation and liner installation, and plane-strain conditions along the axis of the tunnel.

A number of examples are presented, which are solved using the analytical solution and the commercial Finite Element code ABAQUS. The results show that the analytical solution provides results that are comparable to those obtained using the numerical method, which indicates that the analytical solution is correct.

Existing analytical solutions for isotropic rock, e.g., the relative stiffness method, indicate that stresses in the rock and in the liner strongly depend on the magnitude of the far-field loading, tunnel radius and thickness, and stiffness of the liner. The new solution for anisotropic rock has shown that the direction of the far-field loading with

Program, under grant CMS- 0856296. This support is gratefully acknowledged.

Appendix I: Derivatives of Stress Functions

This Appendix contains the derivatives of the stress functions associated with problems II and III, as defined in Fig. 4.

Problem II:

$$\begin{aligned} \phi'_1 &= \frac{1}{\mu_1 - \mu_2} \frac{\sigma_h - \mu_2 \sigma_v + (1 + \mu_2) i \tau_{vh}}{(1 + \mu_1) \zeta_1^2 - 1 + \mu_1} \\ \phi'_2 &= -\frac{1}{\mu_1 - \mu_2} \frac{\sigma_h - \mu_1 \sigma_v + (1 + \mu_1) i \tau_{vh}}{(1 + \mu_2) \zeta_2^2 - 1 + \mu_2} \end{aligned} \tag{36}$$

Problem III:

$$\begin{aligned} \phi'_1 &= -\frac{1}{2} \frac{1}{(\mu_1 - \mu_2) [(1 + \mu_1) \zeta_1^2 - 1 + \mu_1]} \left\{ [2(1 - \mu_2) \sigma_o + (1 + \mu_2) (\sigma_2^a - \tau_2^a + i \sigma_2^b + i \tau_2^b)] + \right. \\ &\quad \left. \sum_{n=3,5,7}^{\infty} [(1 - \mu_2) (\sigma_{n-1}^a + \tau_{n-1}^a + i \sigma_{n-1}^b - i \tau_{n-1}^b) + (1 + \mu_2) (\sigma_{n+1}^a - \tau_{n+1}^a + i \sigma_{n+1}^b + i \tau_{n+1}^b)] \frac{1}{\zeta_1^{n-1}} \right\} \\ \phi'_2 &= \frac{1}{2} \frac{1}{(\mu_1 - \mu_2) [(1 + \mu_2) \zeta_2^2 - 1 + \mu_2]} \left\{ [2(1 - \mu_1) \sigma_o + (1 + \mu_1) (\sigma_2^a - \tau_2^a + i \sigma_2^b + i \tau_2^b)] + \right. \\ &\quad \left. \sum_{n=3,5,7}^{\infty} [(1 - \mu_1) (\sigma_{n-1}^a + \tau_{n-1}^a + i \sigma_{n-1}^b - i \tau_{n-1}^b) + (1 + \mu_1) (\sigma_{n+1}^a - \tau_{n+1}^a + i \sigma_{n+1}^b + i \tau_{n+1}^b)] \frac{1}{\zeta_2^{n-1}} \right\} \end{aligned} \tag{37}$$

respect to the axis of elastic symmetry of the rock and the values of the elastic properties of the rock are additional parameters that need to be considered, as they may have a large effect on the solution. The results show that stresses and displacements do not change if the tunnel is placed above or below the water table as long as the total far-field stresses are the same. Uniform loading, in anisotropic rock, does not induce uniform displacements or stresses in the liner as it occurs with isotropic rock, and so a tunnel liner in anisotropic rock will always be subjected to bending.

The tunnel response does change with the type of loading, i.e., static or seismic (seismic loading in the paper is approximated with a quasi-static loading) when the tunnel is above or below the water table. If the rock is saturated, liner displacements and stresses seem to be more uniform than when the rock is dry or when no excess pore pressures are generated.

Acknowledgments The research has been supported in part by the US National Science Foundation, Civil, Mechanical, and Manufacturing Innovation Division, Geomechanics and Geomaterials

where μ_1 and μ_2 are the modulus of the complex roots (i.e., they are real numbers).

Appendix II: Displacements at Tunnel Perimeter

This Appendix includes expressions for the displacements of the rock at the tunnel perimeter, i.e., at $r = r_o$, and of the liner.

Problem II:

$$\begin{aligned} U_x &= \frac{r_o}{\mu_1 - \mu_2} \left\{ (\mu_1^2 A_1 + A_2) [(\sigma_h - \mu_2 \sigma_v) \cos \theta + (1 + \mu_2) \tau_{vh} \sin \theta] - (\mu_2^2 A_1 + A_2) \right. \\ &\quad \left. \times [(\sigma_h - \mu_1 \sigma_v) \cos \theta + (1 + \mu_1) \tau_{vh} \sin \theta] \right\} \\ U_y &= \frac{r_o}{\mu_1 - \mu_2} \left\{ \left(\mu_2 A_2 + \frac{A_3}{\mu_2} \right) [(\mu_1 \sigma_v - \sigma_h) \sin \theta + (1 + \mu_1) \tau_{vh} \cos \theta] - \right. \\ &\quad \left. \left(\mu_1 A_2 + \frac{A_3}{\mu_1} \right) [(\mu_2 \sigma_v - \sigma_h) \sin \theta + (1 + \mu_2) \tau_{vh} \cos \theta] \right\} \end{aligned} \tag{38}$$

Problem III:

$$\begin{aligned}
 U_x = & -\frac{1}{2} \frac{r_o}{(\mu_1 - \mu_2)} (\mu_1^2 A_1 + A_2) \left\{ [2(1 - \mu_2)\sigma_o + (1 + \mu_2)(\sigma_2^a - \tau_2^a)] \cos \theta \right. \\
 & + (1 + \mu_2)(\sigma_2^b + \tau_2^b) \sin \theta \\
 & + \sum_{n=3,5,7}^{\infty} \frac{1}{n} [(1 - \mu_2)(\sigma_{n-1}^a + \tau_{n-1}^a) + (1 + \mu_2)(\sigma_{n+1}^a - \tau_{n+1}^a)] \cos n\theta \\
 & \left. + \sum_{n=3,5,7}^{\infty} \frac{1}{n} [(1 - \mu_2)(\sigma_{n-1}^b - \tau_{n-1}^b) + (1 + \mu_2)(\sigma_{n+1}^b + \tau_{n+1}^b)] \sin n\theta \right\} \\
 & + \frac{1}{2} \frac{r_o}{(\mu_1 - \mu_2)} (\mu_2^2 A_1 + A_2) \left\{ [2(1 - \mu_1)\sigma_o + (1 + \mu_1)(\sigma_2^a - \tau_2^a)] \cos \theta \right. \\
 & + (1 + \mu_1)(\sigma_2^b + \tau_2^b) \sin \theta \\
 & + \sum_{n=3,5,7}^{\infty} \frac{1}{n} [(1 - \mu_1)(\sigma_{n-1}^a + \tau_{n-1}^a) + (1 + \mu_1)(\sigma_{n+1}^a - \tau_{n+1}^a)] \cos n\theta \\
 & \left. + \sum_{n=3,5,7}^{\infty} \frac{1}{n} [(1 - \mu_1)(\sigma_{n-1}^b - \tau_{n-1}^b) + (1 + \mu_1)(\sigma_{n+1}^b + \tau_{n+1}^b)] \sin n\theta \right\} \\
 U_y = & -\frac{1}{2} \frac{r_o}{(\mu_1 - \mu_2)} \left(\mu_1 A_2 + \frac{A_3}{\mu_1} \right) \left\{ [2(1 - \mu_2)\sigma_o + (1 + \mu_2)(\sigma_2^a - \tau_2^a)] \sin \theta \right. \\
 & - (1 + \mu_2)(\sigma_2^b + \tau_2^b) \cos \theta \\
 & + \sum_{n=3,5,7}^{\infty} \frac{1}{n} [(1 - \mu_2)(\sigma_{n-1}^a + \tau_{n-1}^a) + (1 + \mu_2)(\sigma_{n+1}^a - \tau_{n+1}^a)] \sin n\theta \\
 & - \sum_{n=3,5,7}^{\infty} \frac{1}{n} [(1 - \mu_2)(\sigma_{n-1}^b - \tau_{n-1}^b) + (1 + \mu_2)(\sigma_{n+1}^b + \tau_{n+1}^b)] \cos n\theta \left. \right\} \\
 & + \frac{1}{2} \frac{r_o}{(\mu_1 - \mu_2)} \left(\mu_2 A_2 + \frac{A_3}{\mu_2} \right) \left\{ [2(1 - \mu_1)\sigma_o + (1 + \mu_1)(\sigma_2^a - \tau_2^a)] \sin \theta \right. \\
 & - (1 + \mu_1)(\sigma_2^b + \tau_2^b) \cos \theta \\
 & + \sum_{n=3,5,7}^{\infty} \frac{1}{n} [(1 - \mu_1)(\sigma_{n-1}^a + \tau_{n-1}^a) + (1 + \mu_1)(\sigma_{n+1}^a - \tau_{n+1}^a)] \sin n\theta \\
 & - \sum_{n=3,5,7}^{\infty} \frac{1}{n} [(1 - \mu_1)(\sigma_{n-1}^b - \tau_{n-1}^b) + (1 + \mu_1)(\sigma_{n+1}^b + \tau_{n+1}^b)] \cos n\theta \left. \right\} \tag{39}
 \end{aligned}$$

where μ_1 and μ_2 are the modulus of the complex roots (i.e., real numbers). The values of A_1 , A_2 , and A_3 are

$$\begin{aligned}
 A_1 &= \alpha_1 \\
 A_2 &= \alpha_2 \\
 A_3 &= \alpha_3 \tag{40}
 \end{aligned}$$

For saturated rock and undrained conditions

$$\begin{aligned}
 A_1 &= \alpha_1 - \frac{\beta_1^2}{\beta_3} \\
 A_2 &= \alpha_2 + \frac{\beta_1 \beta_2}{\beta_3} \\
 A_3 &= \alpha_3 - \frac{\beta_2^2}{\beta_3} \tag{41}
 \end{aligned}$$

Liner:

$$\begin{aligned}
 U_x^s = & \frac{1 - \nu_s^2}{E_s (I_s + r_o^2 A_s)} r_o^4 \sigma_o \cos \theta - C \sin \theta \\
 & + \frac{11 - \nu_s^2}{2 E_s I_s} r_o^2 \left\{ \frac{1}{12} [(2\sigma_2^a - \tau_2^a) r_o^2 - 3 \frac{I_s}{A_s} \tau_2^a] \cos \theta \right. \\
 & + \frac{1}{12} [(2\sigma_2^b + \tau_2^b) r_o^2 + 3 \frac{I_s}{A_s} \tau_2^b] \sin \theta \\
 & + \sum_{n=3,5,7}^{\infty} \left[\left(\frac{(n-1)\sigma_{n-1}^a - \tau_{n-1}^a}{n^2(n-1)^2(n-2)} + \frac{(n+1)\sigma_{n+1}^a - \tau_{n+1}^a}{n^2(n+1)^2(n+2)} \right) r_o^2 \right. \\
 & + \frac{I_s}{A_s} \left(\frac{\tau_{n-1}^a}{(n-1)^2} - \frac{\tau_{n+1}^a}{(n+1)^2} \right) \left. \right] \cos n\theta \\
 & + \sum_{n=3,5,7}^{\infty} \left[\left(\frac{(n-1)\sigma_{n-1}^b + \tau_{n-1}^b}{n^2(n-1)^2(n-2)} + \frac{(n+1)\sigma_{n+1}^b + \tau_{n+1}^b}{n^2(n+1)^2(n+2)} \right) r_o^2 \right. \\
 & - \frac{I_s}{A_s} \left(\frac{\tau_{n-1}^b}{(n-1)^2} - \frac{\tau_{n+1}^b}{(n+1)^2} \right) \left. \right] \sin n\theta \left. \right\} \\
 U_y = & \frac{1 - \nu_s^2}{E_s (I_s + r_o^2 A_s)} r_o^4 \sigma_o \sin \theta + C \cos \theta \\
 & + \frac{11 - \nu_s^2}{2 E_s I_s} r_o^2 \left\{ -\frac{1}{12} [(2\sigma_2^a - \tau_2^a) r_o^2 - 3 \frac{I_s}{A_s} \tau_2^a] \sin \theta \right. \\
 & + \frac{1}{12} [(2\sigma_2^b + \tau_2^b) r_o^2 + 3 \frac{I_s}{A_s} \tau_2^b] \cos \theta \\
 & + \sum_{n=3,5,7}^{\infty} \left[\left(\frac{(n-1)\sigma_{n-1}^a - \tau_{n-1}^a}{n^2(n-1)^2(n-2)} - \frac{(n+1)\sigma_{n+1}^a - \tau_{n+1}^a}{n^2(n+1)^2(n+2)} \right) r_o^2 \right. \\
 & + \frac{I_s}{A_s} \left(\frac{\tau_{n-1}^a}{(n-1)^2} + \frac{\tau_{n+1}^a}{(n+1)^2} \right) \left. \right] \sin n\theta \\
 & - \sum_{n=3,5,7}^{\infty} \left[\left(\frac{(n-1)\sigma_{n-1}^b + \tau_{n-1}^b}{n^2(n-1)^2(n-2)} - \frac{(n+1)\sigma_{n+1}^b + \tau_{n+1}^b}{n^2(n+1)^2(n+2)} \right) r_o^2 \right. \\
 & - \frac{I_s}{A_s} \left(\frac{\tau_{n-1}^b}{(n-1)^2} + \frac{\tau_{n+1}^b}{(n+1)^2} \right) \left. \right] \cos n\theta \left. \right\} \tag{42}
 \end{aligned}$$

where C is a constant to be determined in the same manner as the other constants.

References

ABAQUS (2009) User's Manual, Version 6.8–1. Dassault Systemes Simulia Corp, Providence

Bobet A (2001) Analytical solutions for shallow tunnels in saturated ground. ASCE J Eng Mech 127(12):1258–1266

Bobet A (2003) Effect of pore water pressure on tunnel support during static and seismic loading. Tunn Undergr Space Technol 18:377–393

- Bobet A (2007) Ground and liner stresses due to drainage conditions in deep tunnels. *Felsbau* 25(4):42–47
- Bobet A (2009a) Characteristic curves for deep circular tunnels in poroplastic rock. *Rock Mech Rock Eng* (in press)
- Bobet A (2009b) Drained and undrained response of deep tunnels subjected to far-field shear loading. *Tunn Undergr Sp Technol* (in press)
- Bobet A, Nam S (2007) Stresses around pressure tunnels with semi-permeable liners. *Rock Mech Rock Eng* 40(3):287–315
- Bobet A, Fernandez G, Huo H, Ramirez J (2008) A practical procedure to estimate seismic-induced deformations of shallow rectangular structures. *Can Geotech J* 45(7):923–938
- Carranza-Torres C (2004) Elasto-plastic solution of tunnel problems using the generalized form of the Hoek-Brown failure criterion. *Int J Rock Mech Min Sci* 34(3–4):075
- Carranza-Torres C, Fairhurst C (2000) Application of the convergence-confinement method design to rock masses that satisfy the Hoek-Brown failure criterion. *Tunn Undergr Space Technol* 15(2):187–213
- Carranza-Torres C, Zhao J (2009) Analytical and numerical study of the effect of water pore pressure on the mechanical response of cylindrical lined tunnels in elastic and elasto-plastic porous media. *Int J Rock Mech Min Sci* 46(3):531–547
- Cheng AH-D (1998) On generalized plan strain poroelasticity. *Int J Rock Mech Min Sci* 35(2):183–193
- Detournay E, Cheng AH-D (1993). Fundamentals of poroelasticity. In: Hudson JA (ed.) *Comprehensive rock engineering: principles, practice and projects*. Pergamon Press, Oxford, UK, vol 2, pp 113–171
- Einstein HH, Schwartz CW (1979) Simplified analysis for tunnel supports. *ASCE J Geotech Eng Div* 105(GT4):499–518
- Exadaktylos GE, Stavropoulou MC (2002) A closed-form elastic solution for stresses and displacements around tunnels. *Int J Rock Mech Min Sci* 39(7):905–916
- Fernández G, Tirso A, Alvarez A Jr (1994) Seepage-induced effective stresses and water pressures around pressure tunnels. *J Geotech Eng ASCE* 120(1):108–128
- Flügge W (1966) *Stresses in Shells*. Springer, New York
- Giraud A, Homand F, Labiouse V (2002) Explicit solutions for the instantaneous undrained contraction of hollow cylinders and spheres in porous elastoplastic medium. *Int J Numer Anal Methods Geomech* 26:231–258
- Hefny AM, Lo KY (1999) Analytical solutions for stresses and displacements around tunnels driven in cross-anisotropic rocks. *Int J Numer Anal Methods Geomech* 23:161–177
- Hendron AJ, Fernández G (1983) Dynamic and static design considerations for underground chambers. In: Howard TR (ed) *Seismic design of embankments and caverns*, ASCE, NY, pp 157–197
- Huo H, Bobet A, Fernández G, Ramírez J (2006) Analytical solution for deep rectangular structures subjected to far-field shear stresses. *Tunn Undergr Space Technol* 21(6):613–625
- Lee S-W, Jung J-W, Nam S-W, Lee I-M (2006) The influence of seepage forces on ground reaction curve of circular opening. *Tunn Undergr Space Technol* 22:28–38
- Lekhnitskii SG (1963) *Theory of elasticity of an anisotropic elastic body*. Holden-Day, Inc., San Francisco
- Merritt JL, Monsees JE, Hendron AJ Jr (1985) Seismic design of underground structures. In: Mann CD, Kelley MN (eds) *Proceedings of the rapid excavation and tunneling conference (RETC)*. Society of Mining Engineers of the American Institute of Mining, Metallurgical, and Petroleum Engineers, New York, pp 104–131
- Monsees JE, Merritt JL (1988) Seismic modeling and design of underground structures. *Numerical methods in geomechanics*, Innsbruck 1988. In: Swoboda G (ed) *Proceedings of the sixth international conference on numerical methods in geomechanics*. Balkema, Rotterdam, Holland, pp 1833–1842
- Nam S, Bobet A (2006) Liner stresses in deep tunnels below the water table. *Tunn Undergr Space Technol* 21(6):626–635
- Peck RB (1969) Deep excavations and tunneling in soft ground. In: *Proceedings 7th international conference on soil mechanics and foundation engineering, State-of-the-Art Volume*. The Sociedad Mexicana de Mecánica de Suelos, Mexico City, Mexico, pp 225–290
- Peck RB, Hendron AJ, Mohraz B (1972) State of the art of soft-ground tunneling. In: Lane KS, Garfield LA (eds) *Proceedings of the north american rapid excavation and tunneling conference*. Society of Mining Engineers of the American Institute of Mining, Metallurgical, and Petroleum Engineers, pp 259–286
- Penzien J (2000) Seismically induced raking of tunnel linings. *Earthq Eng Struct Dyn* 29:683–691
- Sharan SK (2003) Elastic-brittle-plastic analysis of circular openings in Hoek-Brown media. *Int J Rock Mech Min Sci* 40:817–824
- Sharan SK (2005) Exact and approximate solutions for displacements around circular openings in elastic-brittle-plastic Hoek-Brown rock. *Int J Rock Mech Min Sci* 42:542–549
- Strack OE, Verruijt A (2002) A complex variable solution for a deforming buoyant tunnel in a heavy elastic half-plane. *Int J Numer Anal Methods Geomech* 26:1235–1252
- Tonon F, Amadei B (2002) Effect of elastic anisotropy on tunnel wall displacements behind a tunnel face. *Rock Mech Rock Eng* 35(3):141–160
- Verruijt A (1997) A complex variable solution for a deforming circular tunnel in an elastic half-plane. *Int J Numer Anal Methods Geomech* 21:77–89
- Verruijt A (1998) Deformations of an elastic half plane with a circular cavity. *Int J Solids Struct* 35(21):2795–2804
- Verruijt A, Booker JR (1996) Surface settlements due to deformation of a tunnel in an elastic half plane. *Géotechnique* 46:753–756
- Wang JN (1993) *Seismic design of tunnels. A State-of-the-Art Approach*. Monograph 7, Parsons Brickerhoff Quade & Douglas, Inc., New York
- Wang Y (1996) Ground response of circular tunnel in poorly consolidated rock. *J Geotech Eng* 122(9):703–708
- Wang HF (2000) *Theory of linear poroelasticity with applications to geomechanics and hydrogeology*. Princeton University Press, Princeton